Membrane mimetic thermal proteome profiling (MM-TPP) towards mapping membrane protein-ligand dynamic interactions

Rupinder Singh Jandu[1], Ashim Bhattacharya[1], Frank Antony[1], Mohammed Al-Seragi[1], Hiroyuki Aoki[2], Mohan Babu[2], Franck Duong van Hoa[1]*

[1] Department of Biochemistry and Molecular Biology, Life Sciences Institute, University of British Columbia, Vancouver, British Columbia, Canada.

[2] Department of Biochemistry, University of Regina, Regina, Saskatchewan, Canada.

*Correspondence to: fduong@mail.ubc.ca

Abstract

Integral membrane proteins (IMPs) are central targets for small-molecule therapeutics, yet robust, unbiased, and detergent-free approaches to assess their on- and off-target interactions remain limited. Previously, we introduced the Peptidisc membrane mimetic (MM) for water-soluble stabilization of the membrane proteome and interactome (Carlson et al., eLife, 2019). In this work, we combine the Peptidisc with thermal proteome profiling (TPP) to establish membrane mimetic thermal proteome profiling (MM-TPP), a method that enables proteome-wide mapping of membrane protein–ligand interactions. Using a membrane protein library derived from mouse liver tissue, we detected the specific effects of ATP and orthovanadate on the thermal stability of ATP-binding cassette (ABC) transporters, as well as stability shifts driven by the hydrotropic effect of ATP and its by-products on G protein–coupled receptors (GPCRs). In contrast, detergent-based TPP (DB-TPP) with ATP–VO_4 failed to yield specific enrichment of ATP-binding proteins, underscoring the unique capacity of MM-TPP. To further validate the approach, we demonstrated the ability of MM-TPP to detect specific ligand-induced stabilization

of cognate targets, exemplified by the selective thermal stabilization of the P2RY12 receptor by 2-methylthio-ADP. Together, these findings position MM-TPP as a robust platform for uncovering both on- and off-target effects of small molecules, providing insights into the druggable membrane proteome and its stability in consequence of changing dynamic ligands.

Introduction

Integral membrane proteins (IMPs) are essential to numerous cellular functions, including signal transduction, cell-cell recognition, and the transport of nutrients and ions across cellular membranes (Boulos et al., 2023). Although comprising only 20 to 30% of the human genome, they represent nearly two-thirds of druggable targets due to their significant impact on cellular physiology and their exposure to the cell surface. This prevalence highlights the critical nature of IMPs in pharmacology (Bakheet and Doig, 2009; Fagerberg et al., 2010; Helbig et al., 2010; Santos et al., 2017). However, studying the interactions between small-molecule drugs and membrane proteins poses unique challenges, primarily due to the low abundance and hydrophobic characteristics of these proteins, which complicate their characterization and analysis.

Proteomics-based technologies have become powerful tools for identifying protein–ligand interactions (Aebersold and Mann, 2016; Li et al., 2016). Among these, affinity purification mass spectrometry (AP-MS) uses chemical compounds covalently attached to an affinity matrix to capture target proteins, allowing for detailed characterization of their

interactions (Dunham et al., 2012; Kawatani and Osada, 2014). Another approach, drug affinity responsive target stability (DARTS), leverages ligand-induced conformational changes detected through limited proteolysis, offering insights into the dynamic nature of protein–ligand interactions (Lomenick et al., 2009; Pai et al., 2015). In addition to AP-MS and DARTS, thermal proteome profiling (TPP) has emerged as a complementary approach for studying protein–ligand interactions (Lambos et al, 2025). Derived from the cellular thermal shift assay, TPP enables the detection of ligand-induced conformational changes by assessing protein stability under heat stress (Molina et al., 2013; Savitski et al., 2014). Its relatively straightforward implementation has made it a popular choice in drug screening campaigns. However, TPP typically relies on cytosolic extracts and often overlooks pharmaceutically relevant transmembrane proteins (Franken et al., 2015; Mateus et al., 2020; Lambos et al., 2025).

To expand these techniques to membrane proteome coverage, detergent-based solubilization has been widely used (Huber et al., 2015; Kalxdorf et al., 2021; Reinhard et al., 2015). However, even mild detergents can disrupt native protein structures or drug associations, leading to artifacts that complicate drug target identification (Berlin et al., 2023; Yang et al., 2014; Ye et al., 2023). While crucial for solubilizing membrane proteins and enabling structural and functional studies (O'Malley et al., 2011; Allison et al., 2015; Beckner et al., 2020), detergents remain as we show here largely incompatible with workflows like TPP due to mass spectrometry (MS) limitations (Brough et al., 2024; Antony et al., 2025).

To overcome the limitations associated with detergent use, a variety of MMs have been developed to maintain membrane proteins in a water-soluble, native-like state (Denisov and

Sligar, 2016; Dörr et al., 2014; Young, 2023). Among these, the Peptidisc has emerged as a versatile, self-assembling scaffold characterized by its "one-size-fits-all" property, capable of stabilizing IMPs of diverse sizes and topologies (Carlson et al., 2018). This adaptability has enabled the comprehensive isolation of membrane proteomes from both bacterial and mammalian sources, yielding so-called Peptidisc libraries that are directly compatible with downstream MS workflows (Antony et al., 2024; Carlson et al., 2019; Zhao et al., 2023). In addition to MS compatibility, these libraries also capture and stabilize IMPs in their functional states while preserving their interactomes and lipid allosteric modulators, thus enabling a more comprehensive analysis of membrane protein dynamics and ligand interactions (Angiulli et al., 2020; Carlson et al., 2019; Jandu et al., 2024; Urner et al., 2022).

Building on this foundation, we thought to integrate the Peptidisc into the TPP workflow, introducing a straightforward and detergent-free approach termed membrane mimetic TPP (MM-TPP). Here we apply the MM-TPP workflow to bacterial and mouse liver membrane proteomes, demonstrating its ability to detect ATP-binding proteins, including ABC transporters, G protein–coupled receptors (GPCRs), and multi-subunit complexes. Notably, this approach is sensitive enough to capture interactions mediated by ATP by-products, offering critical insights into both system-wide and ligand-specific dynamics—factors that are essential to consider in small-molecule drug development.

Results and Discussion

The MM-TPP workflow is illustrated in **Figure 1**. Initially, the detergent-solubilized membrane fraction is reconstituted into Peptidisc libraries, as described in previous studies (Antony et al., 2024; Carlson et al., 2019; Zhao et al., 2023). The library is subsequently divided into two aliquots: one exposed to the ligand of interest (treatment), and the other treated with ddH_2O (control). Afterward, the samples are heated for three minutes to facilitate protein denaturation and precipitation. The soluble fraction is then isolated via ultracentrifugation and analyzed by liquid chromatography–tandem mass spectrometry (LC-MS/MS). Proteins exhibiting significant stabilization or destabilization are identified using the methodology outlined by Zhang et al. (2020), in which proteins that meet defined fold-difference thresholds between triplicate treatment and control groups are considered highly probable ligand binders.

As a validation step for the MM-TPP approach, we determined the thermal stability of the purified and Peptidisc-reconstituted bacterial ABC transporter MsbA in the presence of ATP and vanadate (VO_4). Vanadate is a potent inhibitor of the ABC transporter family and, upon binding with ATP, stabilizes the transporter in a specific conformation (Lyu et al., 2022). Consistent with this mechanism, SDS-PAGE analysis revealed increased thermal stability of MsbA in the presence of these ligands (**Figure 2A** and **Supplementary Figure 1**). To extend this observation to a more native context, we further assessed the effect of ATP–VO_4 on a Peptidisc library derived from wild-type *E. coli*, where MsbA is present at endogenous expression levels (**Figure 2B**). In the control sample, MsbA peptide abundance progressively decreased at 51, 56, and 61 °C relative to the bulk proteome. In contrast, in the presence of ATP-VO_4, MsbA was significantly stabilized at 51 °C and above (**Figure 2C**), demonstrating that our approach can detect thermal stabilization even in proteins expressed at low endogenous levels.

Notably, at 61 °C, the volcano plot revealed that MsbA stabilization coincided with that of two other integral membrane proteins (IMPs), FtsK and LolC (**Figure 2D**). FtsK, one of the longest membrane proteins in E. coli (1329 amino acids), belongs to the AAA ATPase family, while LolC is the membrane transport domain of the soluble ABC subunit LolD (Sharma et al., 2021). In contrast, DgkA, which is a small diacylglycerol kinase comprising 122 amino acids, exhibited destabilization under the same conditions (**Figure 2D**) (Li et al., 2015; Zheng and Jia, 2013). Collectively, these results validate MM-TPP as a robust and straightforward method for identifying ATP binders within complex mixtures of soluble and integral membrane proteins.

We next applied the MM-TPP workflow to mouse liver tissue, where drug screening for cell surface IMPs is particularly relevant. As expected, the total number of proteins identified decreased following heat treatment (**Figure 3A**). Notably, in this detergent-free environment, this reduction affected soluble and membrane proteins equally, with the proportion of IMPs remaining stable across temperatures—approximately 48% (**Supplemental Table 1**). We then performed MM-TPP in the presence of ATP-VO_4 (**Figure 3B**). Consistent with results from the *E. coli* library, most proteins exhibited increased thermal stability upon ATP-VO_4 treatment, as indicated by the rightward shift of data points in the plot. Recent studies suggest that ATP can function as a natural hydrotrope, influencing the global stability of protein populations by interacting with thermally sensitive regions (Ou et al., 2021; Patel et al., 2017). Important to this study and as expected, GO-term analysis of significantly stabilized IMPs revealed enrichment in functions related to nucleoside-phosphate binding and primary active transport (**Figure 3C**). Supporting this, thermal stability profiles across different temperatures confirmed a marked sensitivity of ABC transporters. Among the ten ABC transporters identified in the liver library,

eight showed significant thermal stabilization in the presence of ATP-VO_4 at one or more temperature points (**Table 1** and **Figure 3D**). Besides ABC transporters, the BCS1L protein exhibited a remarkable ~30-fold increase in stability, which was further enhanced by AMP-PNP (**Figure 3E** and **Supplementary Figure 2**). This enhanced stabilization is consistent with recent structural studies demonstrating substantial conformational changes in the heptameric BCS1L complex upon binding of this non-hydrolyzable ATP analog (Pan et al., 2023; Tang et al., 2020; Zhan et al., 2024).

To further assess the effectiveness of MM-TPP, we directly compared its performance to a detergent-based TPP assay (DB-TPP) at 51 °C. In both workflows, crude membrane fractions from mouse liver were solubilized in 1% DDM to extract membrane proteins. However, while MM-TPP involves reconstitution of solubilized proteins into Peptidiscs before heat treatment, the DB-TPP workflow omits this step, keeping the proteins in detergent solution throughout. Following thermal treatment, DB-TPP also includes an additional detergent removal step for MS analysis. This side-by-side comparison revealed key differences in the TTP profiles. Overall, DB-TPP provided broader proteome coverage, including a greater number of soluble proteins identified (**Table 2**). In contrast, in the MM-TPP workflow, soluble proteins were actively depleted during Peptidisc reconstitution, resulting in an IMP-enriched proteome. Crucially, at 51 °C, 7.4% of all identified proteins and 6.4% of differentially stabilized proteins in the DB-TPP dataset were annotated as ATP-binding, indicating that the apparent differential stabilization is likely stochastic rather than driven by specific ligand binding (**Figure 4A**). By comparison, in MM-TPP, 9.3% of all identified proteins and 17% of differentially stabilized proteins were

annotated as ATP-binding, demonstrating selective enrichment for ATP-VO_4-mediated stabilization events **(Figure 3B**).

Beyond demonstrating improved selectivity for ATP-VO_4-mediated stabilization, we next asked whether MM-TPP could also resolve more selective ligand–protein interactions. To test this, we applied the method using 2-methylthio-ADP (2-MeS-ADP), a well-characterized agonist of the P2RY12 receptor (Zhang et al., 2014). MM-TPP revealed clear and reproducible thermal stabilization of P2RY12, showing more than a sixfold increase in stability at both 51 °C and 57 °C ($-\log_{10} p > 5.97$; **Figure 4B** and **Figure S4**). Notably, no other proteins, including the structurally related but non-responsive P2RY6 receptor, exhibited comparable stabilization, underscoring MM-TPP's ability to detect highly specific ligand–receptor interactions amidst a complex membrane proteome.

Next to these highly specific receptor–ligand interactions, we also observed a broader spectrum of thermal stabilization events that lacked direct annotation to ATP binding. For instance, a substantial proportion of IMPs without known ATP-binding function were still significantly stabilized in the presence of ATP–VO_4. For example, among the 178 IMPs that passed the significance threshold, approximately 43% were annotated with GO terms related to nucleic acid/nucleotide binding, GTP binding, phosphate binding, and other related functions **(Figure 5A**). Some of these IMPs may achieve stabilization indirectly through interactions with ATP-binding partners, as illustrated by the LolC/LolD complex reported above (**Figure 2D**). Others may exhibit off-target stabilization effects, potentially due to ATP metabolites such as ADP, AMP, or inorganic phosphate, which are known to influence protein conformation and

stability. This scenario is exemplified by the purinergic receptor P2RY6, a GPCR that responds preferentially to ADP rather than ATP (von Kügelgen and Hoffmann, 2016), which showed the highest differential thermal stabilization among all IMPs at 56 °C (**Supplementary File**). Similarly, P2RY12, a member of the same GPCR family, showed significant stabilization across 56, 60, and 64 °C (**Supplemental File**), consistent with its known preference for ADP (Entsie et al., 2023; Zhang et al., 2014). Supporting this interpretation, neither receptor exhibited thermal stabilization in the presence of the non-hydrolyzable ATP analog AMP-PNP (**Figure 5B**). Conversely, the trimeric ATP-gated cation channel P2RX4 showed significant destabilization in response to ATP–VO_4 at 51 and 64 °C (**Figure 3B**) and AMP-PNP at 56 and 64 °C (**Figure 5C**), consistent with previous reports highlighting the unique ATP sensitivity of P2RX family members compared to the P2RY family (Carnero Corrales et al., 2021; Thompson et al., 2021).

Among all observed side-effects, the most striking stabilization was detected for the FAD-containing monoamine oxidase B (Mao-B) at 64 °C **(Supplementary Figure 3**). To explore the potential basis for this off-target effect, we used AlphaFold3 to model the binding of ATP and its derivatives within the FAD-binding pocket of Mao-B (Abramson et al., 2024). Interestingly, the best-fitting models were obtained for ADP and AMP (pLDDT > 90), while ATP yielded the lowest confidence score (**Figure 5D**). Although this computational result remains hypothetical, it offers a plausible structural rationale that warrants further experimental validation.

Finally, to validate the robustness of these findings, we assessed the reproducibility of MM-TPP by repeating the ATP–VO_4 experiment at 51 °C using data-independent acquisition

(DIA) (**Supplementary Figure 5**), in contrast to the data-dependent acquisition (DDA) employed initially. The results were highly consistent with the previous dataset. Overall, 7.8% of all identified proteins were annotated as ATP-binding, with this proportion rising to 17% among proteins exhibiting a $\log_2$ fold change greater than 0.5—mirroring the enrichment observed in the DDA-based analysis. Notably, BCS1L and SLC27A2 displayed strong thermal stabilization ($\log_2$ fold change > 1), while several ABC transporters, including ABCB11, ABCG2, ABCD3, ABCG8, and ABCA1, showed intermediate stabilization ($\log_2$ fold changes between 0.5 and 1). In line with earlier results, P2RX4 was again significantly destabilized ($\log_2$ fold change < –1). These findings confirm that MM-TPP produces consistent and reproducible profiles of protein stabilization and destabilization across distinct MS acquisition strategies, further supporting its utility for ligand engagement studies in complex membrane proteomes.

Together, these results validate the integration of Peptidisc libraries into TPP for broad-scale detection of membrane protein–ligand interactions. MM-TPP not only enhances the recovery and stability of IMPs but also enables direct profiling of membrane proteomes from native tissues and organs. This preserves critical biological features, such as endogenous protein expression levels, native protein–protein interactions, post-translational modifications, and tissue-specific isoforms, that are often disrupted in traditional cell culture systems (Kwasnik et al., 2016; Perez-Perri et al., 2023).

Although the Peptidisc workflow does not bypass the need for initial detergent solubilization, it eliminates key downstream limitations associated with detergent-based methods. In particular, MM-TPP preserves ligand binding and is fully compatible with mass

spectrometry, unlike many detergent-based workflows where residual detergent can interfere with both ligand interactions and MS sensitivity (Brough et al., 2024; Lambos et al., 2025). As such, MM-TPP is inherently complementary to detergent-based approaches while offering clear advantages for downstream proteomic analyses. To further expand its applicability, future studies could explore a broader range of nucleotide analogs, including antagonists such as TNP-ATP or ATPγS, and clinically relevant small molecules, such as the CFTR modulator VX-809. These applications would further underscore MM-TPP's pharmacological potential in profiling membrane protein function and drug interactions.

While challenges remain, such as maintaining physiological signaling contexts, integrating MMs like Peptidiscs early in drug discovery offers a powerful strategy. MM-TPP captures both direct target engagement and off-target effects from parent compounds or their metabolites, providing functional insights into ligand dynamics and specificity, which are important considerations in early-stage drug development and safety profiling.

Methods

Preparation of *Escherichia coli* crude membranes

Wild-type *Escherichia coli* BL21 (DE3) was grown in 1 L of LB medium. After 3 hours, cells were harvested by low-speed centrifugation (6000g, 6 min) and resuspended in Buffer A (50 mM Tris-HCl pH 7.8, 100 mM NaCl, 10% Glycerol) supplemented with 1 mM phenylmethylsulfonyl fluoride (1 mM). Cells were lysed through a microfluidizer (Microfluidics; 3 passes at 15,000 psi at 4 °C). Unbroken cells and large aggregates were removed by low-speed centrifugation (6000g,

6 min). The crude membrane fraction was isolated by ultracentrifugation (100000g, 45 min, 4 °C, Beckman Coulter rotor Ti70). Membranes were resuspended in Buffer A at 5 mg/mL and stored at -80°C for later use.

Expression and purification of His-MsbA for thermal stability assay

Histidine-tagged MsbA (His-MsbA) was expressed, purified, and reconstituted in peptidisc through the on-bead method as described in Angiulli et al. (2020) with slight modifications (Angiulli et al., 2020). Briefly, His-tagged MsbA was produced in *E. coli* BL21(DE3) at 37°C in 1 L of LB medium supplemented with 50 µg/mL kanamycin. The inducer IPTG (0.5 mM) was added during the exponential growth phase (OD_{600nm} ~ 0.4). After 3 hours, cells were harvested by low-speed centrifugation (6000g, 6 min) and resuspended in Buffer A (50 mM Tris-HCl pH 7.8, 100 mM NaCl, 10% Glycerol) supplemented with phenylmethylsulfonyl fluoride (1 mM). Cells were lysed through a microfluidizer (Microfluidics; 3 passes at 15,000 psi at 4°C). Unbroken cells and large aggregates were removed by low-speed centrifugation (6000g, 6 min). The crude membrane fraction containing MsbA was isolated by ultracentrifugation (100000g, 45 min, 4°C, Beckman Coulter rotor Ti70). About 2 mg of MsbA-enriched membranes were solubilized with 1% DDM (w/v) for 30 min at 4°C. The detergent solubilized material was ultracentrifuged (180000g, 15 min, 4°C, Beckman Coulter rotor TLA55) to pellet insoluble material. The supernatant was incubated with Ni-NTA (150 µL) resin for 45 min at 4°C on a tabletop rocker. The resin was sedimented through centrifugation (2000g, 1 min) and washed three times with 1.5mL of Buffer A supplemented with 0.02% DDM and 30mM imidazole. After removing the excess buffer, the beads were resuspended in Buffer A containing Peptidisc peptide (1 mg/mL). The excess peptide was washed away with Buffer A. The protein was eluted with

600 mM imidazole in Buffer A and the concentration was determined through a Bradford reagent.

Thermal stability assay of His-MsbA with ATP-VO_4

Purified His-MsbA (0.5 mg/mL) in Buffer A supplemented with 5 mM $MgCl_2$ and 0.2 mM orthovanadate (VO_4) was separated into two equal volumes designated as treatment and control samples. To the treatment sample ATP-disodium-trihydrate (ATP) was added to a final concentration of 2mM and an equal volume of ddH2O was administered to the control. Samples were incubated at room temperature for 10 minutes prior to aliquoting 50 µL into separate 0.2 µL PCR tubes. These aliquots were subjected to temperatures ranging from 45 - 61°C for three minutes, followed by ultracentrifugation at 180000g for 15 minutes at 4°C to pellet the unfolded proteins. The supernatants were collected, and 10 µL from each sample was analyzed on a 12% SDS-PAGE.

Harvest of *Mus musculus* liver

The C57BL/6 mice were kept in specific pathogen-free conditions and received humane care in compliance with the Canadian Council of Animal Care guidelines, and the animal protocol was approved by the Animal Care Committee of the University of British Columbia. The mouse organs were obtained from female mice. The authors acknowledge that they did not consider the impact of mouse sex at the time of the study design. The mice received standard chow. At the age of 12 weeks, the mice were sacrificed, and the liver was excised and placed in vials with ice-cold sterile phosphate-buffered saline (PBS) until processing.

Mus musculus liver processing and preparation of crude membranes

The excised organs were washed several times in ice-cold PBS to remove the blood and then minced and homogenized in ice-cold hypotonic lysis buffer (10 mM Tris–HCl pH 7.4, 30 mM NaCl, and 1 mM EDTA, 1× cocktail protease inhibitor, and 1 mM PMSF) using a tight-fit metal douncer. All subsequent steps were performed at 4 °C or on ice. After adding 10 mM MgCl2 and 50 μg/mL DNase, the suspension was further dounced and incubated for 10 min. The swollen tissue suspension was lysed using a French press (3 passes at 500 PSI). Unbroken cells and nucleus fraction were removed by low-speed centrifugation (1200g for 10 min). The supernatant was collected and centrifuged at a higher speed (5000g, 10 min) to remove the mitochondrial fraction. The crude membrane fraction was then collected by ultracentrifugation (110000g, 45 min) in a Beckman TLA110 rotor. This membrane pellet was resuspended in 100 μL of 50 mM Tris, pH 7.9, 100 mM NaCl, and 10% glycerol (TSG Buffer) and stored at −80 °C until use.

Preparation of Peptidisc membrane protein library

For Peptidisc library preparation, ∼2 mg of crude membranes (either *Escherichia coli* or *Mus musculus*) was solubilized in 50 mM Tris, pH 7.9, 25 mM NaCl, and 1% DDM (Solubilization Buffer) for 30 min at 4 °C with gentle shaking. The insoluble material was pelleted by ultracentrifugation (180000g, 15 min). The detergent extract (500 μL) was then reconstituted by mixing it with a 3-fold excess (w/w) Peptidisc peptide for 15 min at 4 °C. The sample was rapidly diluted to 15 mL in 50 mM Tris, pH 7.9 and 25 mM NaCl (Buffer A) over a 100 kDa cut-off centrifugal filter. The sample was concentrated (3000g, 10 min) to ∼200 μL. This process was repeated for a total of three rounds of dilution and concentration to deplete DDM to an

approximate concentration of 0.008% to complete Peptidisc reconstitution. The Peptidisc library was immediately used for downstream thermal proteome profiling.

MM-TPP profiling on membrane proteomes

Peptidisc membrane protein library was split into two equal aliquots representing the control and treatment samples. Both the treatment and control groups were supplemented with 5 mM $MgCl_2$ and 0.2 mM VO_4. Treatment samples were then exposed to a final concentration of 2 mM ATP, while the control received an equal volume of ddH_2O. For experiments with AMP-PNP, 2 mM AMP-PNP was substituted in place of ATP. The samples were incubated for 10 minutes at room temperature, divided into four aliquots and transferred into 0.2 mL PCR tubes. Each sample was heated in parallel for 3 minutes to its respective temperature (51-64°C), as previous studies have indicated that a 3–5-minute exposure is optimal for visualizing protein denaturation (Martinez Molina et al., 2013; Mateus et al., 2020). Subsequently, the samples were centrifuged at 180000g for 15 minutes at 4°C, and the supernatant was collected for in-solution digestion.

Detergent-based TPP on membrane proteomes

For detergent-based TPP (DB-TPP), ∼2 mg of crude membranes from *Mus musculus* was solubilized in Solubilization Buffer for 30 min at 4 °C with gentle shaking. The insoluble material was pelleted by ultracentrifugation (180,000g, 15 min). The detergent-solubilized library was split into two equal aliquots representing the control and treatment samples. Both the treatment and control groups were supplemented with 5 mM $MgCl_2$ and 0.2 mM VO_4. Treatment samples were then exposed to a final concentration of 2 mM ATP, while the control received an equal volume of ddH2O. The samples were incubated for 10 minutes at room temperature,

divided into four aliquots and transferred into 0.2 mL PCR tubes. Each sample was heated in parallel for 3 minutes to its respective temperature (51-64°C). Subsequently, the samples were centrifuged at 180000g for 15 minutes at 4°C, and the supernatant was collected for processing as described by Johnston et al. (2022). Briefly, silica beads (9−13 µm diameter) were resuspended in water, washed once with 100% acetonitrile (CAN), rinsed twice with water, and resuspended at 50 mg/mL final. After each wash, the beads were isolated by brief centrifugation at 16,000 × g for 1 min. Crude membranes (~1 mg) were resuspended in ice-cold TS buffer (50 mM Tris-HCl, pH 8.0, 100 mM NaCl) supplemented with 1% (w/v) SDC for 30 min at 4°C with gentle shaking. The detergent extract was clarified by ultracentrifugation (110,000 × g for 15 min at 4°C), and aliquots (100 µg each) were gently vortex-mixed with glass beads (1 mg). CAN was then added to a final concentration of 80%, and samples were centrifuged at 16,000 × g for 5 min. The beads were rinsed three times with 500 µL of 80% ethanol without disturbing the pellet. After a final wash, the beads underwent MS sample preparation and LC-MS/MS analysis.

MS sample preparation and LC-MS/MS analysis

Equal volumes of supernatants from the treatment and control groups were treated with 6 M urea at room temperature for 30 min before reduction with 10 mM fresh dithiothreitol (DTT) for 1 h. Alkylation was performed with 20 mM iodoacetamide (IAA) in the dark at room temperature for 30 min, followed by a second round of reduction via 10 mM DTT for 30 min. The urea was diluted to 1 M with Buffer A. Trypsin digestion was performed with an enzyme/protein ratio of 1:100 at room temperature for 24 h. The tryptic peptides were acidified to pH 3 with 10% formic acid and desalted using hand-packed stage tips of C18 resin. The peptides were eluted with 80% acetonitrile and 0.1% formic acid and were dried by vacuum centrifugation. The analysis of

tryptic peptides was performed in a NanoLC connected to an Orbitrap Exploris mass spectrometer (Thermo Fisher Scientific) was used for the analysis of all samples. The peptide separation was carried out using a Proxeon EASY nLC 1200 System (Thermo Fisher Scientific) fitted with a custom-made C18 column (15 cm x 150 μm ID) packed with HxSil C18 3 μm Resin 100 Å (Hamilton). A gradient of water/acetonitrile/0.1% formic acid was employed for chromatography. The samples were injected into the column and run for 180 minutes at a flow rate of 0.60 μl/min. The peptide separation began with 1% acetonitrile, increasing to 3% in the first 4 minutes, followed by a linear gradient from 3% to 23% acetonitrile over 86 minutes, then another increase from 24% to 80% acetonitrile over 35 minutes, and finally a 35-minute wash at 80% acetonitrile, and then decreasing to 1% acetonitrile for 10 min and kept 1% acetonitrile for another 10 min. The eluted peptides were ionized using positive nanoelectrospray ionization (NSI) and directly introduced into the mass spectrometer with an ion source temperature set at 250°C and an ion spray voltage of 2.1 kV. Full-scan MS spectra (m/z 350–2000) were captured in Orbitrap Exploris at a resolution of 120,000 (m/z 400). The automatic gain control was set to 1e6 for full FTMS scans and 5e4 for MS/MS scans. Ions with intensities above 1500 counts underwent fragmentation via nanoelectrospray ionization (NSI) in the linear ion trap. The top 15 most intense ions with charge states of ≥ 2 were sequentially isolated and fragmented using normalized collision energy of 30%, activation Q of 0.250, and an activation time of 10 ms. Ions selected for MS/MS were excluded from further selection for 3 seconds. The Orbitrap Exploris mass spectrometer was operated using Thermo Xcalibur software.

Data analysis in MaxQuant

Raw mass spectrometric files were analyzed in the MaxQuant environment, version 2.4.1.0. The MS/MS spectra were searched using the Andromeda search engine against the UniProt-mouse protein database (UP000000589, December 2021, 55086 entries) and UniProt-*Escherichia coli* protein database (UP000002032, July 2009, 4156 entries). Precursor mass and fragment mass were set with initial mass tolerances of 20 ppm for both the precursor and fragment ions. The search included variable modifications of asparagine/glutamine deamidation, methionine oxidation, and N-terminal acetylation and a fixed modification of carbamidomethyl cysteine. The maximum number of missed cleavages was set at two, and the maximum modifications/peptide and minimum peptide length were set at six amino acids. The UniProt database was also concatenated with an automatically generated reverse database to estimate the false discovery rate (FDR) by using a target decoy search. The false discovery rate (FDR) was set at 0.01 for the peptide spectrum match (PSM) and protein identifications. When identified peptides were all shared between two proteins, they were combined and reported as one protein group. For relative quantification, MaxQuant's label-free quantification method, LFQ, was enabled.

Statistical analysis

Each treatment and control sample were collected from three technical replicates. The ProteinGroups.txt output file from MaxQuant was exported into Perseus v1.6.15.0 for downstream analysis. In-house functions of Perseus were used to identify and remove protein groups from the reverse decoy database, those marked as potential contaminants, or those only identified by a post-translational modification site. The remaining intensity, and label-free quantification (LFQ) intensity were $\log_2$ transformed and normalized to the mean peptidisc peptide intensity value. To identify proteins with significant change in thermal stability, a

Student's t-test was conducted with a within-groups variance, s0, set to 0.1. The test was applied to data filtered for proteins that had at least three valid LFQ intensities in either the treatment or control group. The remaining undefined intensity values were imputed from a normal distribution with a downshift of 1.8 standard deviations from the total sample mean and a width of 0.3 times the sample standard deviation. To determine significantly stabilized or destabilized as a result of ligand exposure, proteins with a $-\log_{10}$ p-value > 1.3 and LFQ peptide intensity $\log_2$ fold change > 1 or <-1 were considered as the direct or indirect candidates of ligand-binders. Only proteins with at least two unique peptides were considered for this calculation, a threshold selected because it aligns with established LC-MS/MS data analysis practices (The et al., 2020; Kurzawa et al., 2020; Reinhard et al., 2015). A table of the unique peptide count for the discussed proteins in the manuscript is provided in Supplemental Table 2. To visualize the temperature-dependent peptide intensity data, the smoothed curves were generated using the Piecewise Cubic Hermite Interpolating Polynomial (PCHIP) method. PCHIP interpolation was applied to the mean intensity values of each experimental group across the temperature gradient. Figures were generated through NumPy, Matplotlib, and Pandas Python coding language.

Ligand binding prediction with AlphaFold3

The web-based AlphaFold server (https://alphafoldserver.com) was utilized to predict ligand binding onto predicted protein structures. Protein peptide sequences were obtained from Uniprot for structure prediction. The resulting output data file was analyzed in Pymol to assess the corresponding B-factor/pLDDT score for each residue interacting with the ligand of interest. The mean pLDDT score from all interacting residues was determined to generate a confidence prediction of ligand binding.

Protein annotation

The protein list obtained from MaxQuant was subjected to a Gene Ontology (GO) term analysis using the UniProtKB database to identify proteins with the GO-term “membrane”. Proteins from this group were extracted in FastA format and the Phobius web server ((http://phobius.sbc.su.se/) was utilized to predict the number of transmembrane segments (TMS). Any protein with at least one TMS was classified as an IMP. Protein with no TMS but with the GO annotation “membrane” was classified as a membrane-associated protein; all other proteins were considered as soluble proteins. To assess molecular functions of significantly stabilized IMPs, the Gene Ontology Molecular Function (‘GO_MF_Direct/GO_MF_FAT’) was used through DAVID Bioinformatics (https://david.ncifcrf.gov/). An EASE score of 0.05 was applied to test for significant GO terms based on a p-value cut-off of 0.05 after Benjamini-Hochberg correction. The gProfiler g:GOSt tool was utilized to reduce redundancy of significantly enriched terms (https://biit.cs.ut.ee/gprofiler/gost).

Data availability statement

The MS-based proteomics data of this study have been deposited to the ProteomeXchange Consortium via the PRIDE partner repository and are available through the identifier PXD055093.

Acknowledgments

This work was supported by the Canadian Institutes of Health Research (CIHR; FDN-154318 to MB and PG20R34019 to FD). RSJ holds a CGS-M scholarship from the Natural Sciences &

Engineering Research Council of Canada (NSERC). AB holds a FYF scholarship from UBC and an Amplify Doctoral Award from Triangle (Training a new generation of researchers in Gastroenterology and liver). MA-S is a recipient of the CBR/LSI Summer Studentship Program.

References

Abramson J, Adler J, Dunger J, Evans R, Green T, Pritzel A, Ronneberger O, Willmore L, Ballard AJ, Bambrick J, Bodenstein SW, Evans DA, Hung C-C, O'Neill M, Reiman D, Tunyasuvunakool K, Wu Z, Žemgulytė A, Arvaniti E, Beattie C, Bertolli O, Bridgland A, Cherepanov A, Congreve M, Cowen-Rivers AI, Cowie A, Figurnov M, Fuchs FB, Gladman H, Jain R, Khan YA, Low CMR, Perlin K, Potapenko A, Savy P, Singh S, Stecula A, Thillaisundaram A, Tong C, Yakneen S, Zhong ED, Zielinski M, Žídek A, Bapst V, Kohli P, Jaderberg M, Hassabis D, Jumper JM. 2024. Accurate structure prediction of biomolecular interactions with AlphaFold 3. *Nature* **630**:493–500. doi:10.1038/s41586-024-07487-w

Aebersold R, Mann M. 2016. Mass-spectrometric exploration of proteome structure and function. *Nature* **537**:347–355. doi:10.1038/nature19949

Allison TM, Reading E, Liko I, Baldwin AJ, Laganowsky A, Robinson CV. 2015. Quantifying the stabilizing effects of protein-ligand interactions in the gas phase. *Nat Commun* **6**:8551 doi: 10.1038/ncomms9551.

Angiulli G, Dhupar HS, Suzuki H, Wason IS, Duong Van Hoa F, Walz T. 2020. New approach for membrane protein reconstitution into peptidiscs and basis for their adaptability to different proteins. *eLife* **9**:e53530. doi:10.7554/eLife.53530

Antony F, Brough Z, Zhao Z, Duong van Hoa F. 2024. Capture of the Mouse Organ Membrane Proteome Specificity in Peptidisc Libraries. *J Proteome Res* **23**:857–867. doi:10.1021/acs.jproteome.3c00825

Antony F, Bhattacharya A, Aoki H, Jandu RS, Abdualkader AM, Al Batran R, Babu M, Duong van Hoa F. 2025. Comparative Evaluation of Solid-Phase and Membrane Mimetic Strategies in Membrane Proteome Coverage and Disease-State Analysis. *bioRxiv* doi: 10.1101/2025.08.25.672181

Bakheet TM, Doig AJ. 2009. Properties and identification of human protein drug targets. *Bioinformatics* **25**:451–457. doi:10.1093/bioinformatics/btp002

Beckner RL, Zoubak L, Hines KG, Gawrisch K, Yeliseev AA. 2020. Probing thermostability of detergent-solubilized CB2 receptor by parallel G protein-activation and ligand-binding assays. *J. Biol. Chem.* **3**:181-190 doi: 10.1074/jbc.RA119.010696.

Berlin E, Lizano-Fallas V, Carrasco del Amor A, Fresnedo O, Cristobal S. 2023. Nonionic Surfactants can Modify the Thermal Stability of Globular and Membrane Proteins Interfering with the Thermal Proteome Profiling Principles to Identify Protein Targets. *Anal Chem* **95**:4033–4042. doi:10.1021/acs.analchem.2c04500

Boulos I, Jabbour J, Khoury S, Mikhael N, Tishkova V, Candoni N, Ghadieh HE, Veesler S, Bassim Y, Azar S, Harb F. 2023. Exploring the World of Membrane Proteins: Techniques and Methods for Understanding Structure, Function, and Dynamics. *Molecules* **28**:7176. doi:10.3390/molecules28207176

Brough Z, Zhao Z, Duong van Hoa F. 2024. From bottom-up to cell surface proteomics: detergents or no detergents, that is the question. *Biochem Soc Trans* **52**:1253-1263 doi: 10.1042/BST20231020.

Carlson ML, Stacey RG, Young JW, Wason IS, Zhao Z, Rattray DG, Scott N, Kerr CH, Babu M, Foster LJ, Duong Van Hoa F. 2019. Profiling the Escherichia coli membrane protein interactome captured in Peptidisc libraries. *eLife* **8**:e46615. doi:10.7554/eLife.46615

Carlson ML, Young JW, Zhao Z, Fabre L, Jun D, Li Jianing, Li Jun, Dhupar HS, Wason I, Mills AT, Beatty JT, Klassen JS, Rouiller I, Duong F. 2018. The Peptidisc, a simple method for stabilizing membrane proteins in detergent-free solution. *eLife* **7**:e34085. doi:10.7554/eLife.34085

Carnero Corrales MA, Zinken S, Konstantinidis G, Rafehi M, Abdelrahman A, Wu Y-W, Janning P, Müller CE, Laraia L, Waldmann H. 2021. Thermal proteome profiling identifies the membrane-bound purinergic receptor P2X4 as a target of the autophagy inhibitor indophagolin. *Cell Chemical Biology* **28**:1750-1757.e5. doi:10.1016/j.chembiol.2021.02.017

Denisov IG, Sligar SG. 2016. Nanodiscs for structural and functional studies of membrane proteins. *Nat Struct Mol Biol* **23**:481–486. doi:10.1038/nsmb.3195

Dörr JM, Koorengevel MC, Schäfer M, Prokofyev AV, Scheidelaar S, van der Cruijsen EAW, Dafforn TR, Baldus M, Killian JA. 2014. Detergent-free isolation, characterization, and functional reconstitution of a tetrameric K+ channel: The power of native nanodiscs. *Proceedings of the National Academy of Sciences* **111**:18607–18612. doi:10.1073/pnas.1416205112

Dunham WH, Mullin M, Gingras A-C. 2012. Affinity-purification coupled to mass spectrometry: Basic principles and strategies. *PROTEOMICS* **12**:1576–1590. doi:10.1002/pmic.201100523

Entsie P, Kang Y, Amoafo EB, Schöneberg T, Liverani E. 2023. The Signaling Pathway of the ADP Receptor P2Y12 in the Immune System: Recent Discoveries and New Challenges. *Int J Mol Sci* **24**:6709. doi:10.3390/ijms24076709

Fagerberg L, Jonasson K, von Heijne G, Uhlén M, Berglund L. 2010. Prediction of the human membrane proteome. *PROTEOMICS* **10**:1141–1149. doi:10.1002/pmic.200900258

Franken H, Mathieson T, Childs D, Sweetman GMA, Werner T, Tögel I, Doce C, Gade S, Bantscheff M, Drewes G, Reinhard FBM, Huber W, Savitski MM. 2015. Thermal proteome profiling for unbiased identification of direct and indirect drug targets using multiplexed quantitative mass spectrometry. *Nat Protoc* **10**:1567–1593. doi:10.1038/nprot.2015.101

Helbig AO, Heck AJR, Slijper M. 2010. Exploring the membrane proteome—Challenges and analytical strategies. *Journal of Proteomics* **73**:868–878. doi:10.1016/j.jprot.2010.01.005

Huber KVM, Olek KM, Müller AC, Tan CSH, Bennett KL, Colinge J, Superti-Furga G. 2015. Proteome-wide drug and metabolite interaction mapping by thermal-stability profiling. *Nat Methods* **12**:1055–1057. doi:10.1038/nmeth.3590

Jandu RS, Yu H, Zhao Z, Le HT, Kim S, Huan T, Hoa FD van. 2024. Capture of endogenous lipids in peptidiscs and effect on protein stability and activity. *iScience* **27**. doi:10.1016/j.isci.2024.109382

Johnston HE, Yadav K, Kirkpatrick JM, Biggs GS, Oxley D, Kramer HB, Samant RS. 2022. Solvent Precipitation SP3 (SP4) Enhances Recovery for Proteomics Sample Preparation without Magnetic Beads. *Anal Chem* **94**:10320–10328. doi:10.1021/acs.analchem.1c04200

Kalxdorf M, Günthner I, Becher I, Kurzawa N, Knecht S, Savitski MM, Eberl HC, Bantscheff M. 2021. Cell surface thermal proteome profiling tracks perturbations and drug targets on the plasma membrane. *Nat Methods* **18**:84–91. doi:10.1038/s41592-020-01022-1

Kawatani M, Osada H. 2014. Affinity-based target identification for bioactive small molecules. *Med Chem Commun* **5**:277–287. doi:10.1039/C3MD00276D

Kwasnik A, Tonry C, Ardle AM, Butt AQ, Inzitari R, Pennington SR. 2016. Proteomes, Their Compositions and Their Sources In: Mirzaei H, Carrasco M, editors. Modern Proteomics

– Sample Preparation, Analysis and Practical Applications, Advances in Experimental Medicine and Biology. Cham: Springer International Publishing. pp. 3–21. doi:10.1007/978-3-319-41448-5_1

Kurzawa N, Becher I, Sridharan S, Franken H, Mateus A, Anders S, Bantscheff M, Huber W, Savitski MM. 2021. A computational method for detection of ligand-binding proteins from dose range thermal proteome profiles. *Nat Commun* **11**:5783 doi: 10.1038/s41467-020-19529-8

Lambos J, Bhattacharya A, Al-Seragi M, Duong F. 2025. Expanding the Reach of Membrane Protein-Ligand Interaction Studies through the integration of Mass Spectrometry and Membrane Mimetics. *Authorea,* doi:10.22541/au.175508838.89786308/v1

Li D, Stansfeld PJ, Sansom MSP, Keogh A, Vogeley L, Howe N, Lyons JA, Aragao D, Fromme P, Fromme R, Basu S, Grotjohann I, Kupitz C, Rendek K, Weierstall U, Zatsepin NA, Cherezov V, Liu W, Bandaru S, English NJ, Gati C, Barty A, Yefanov O, Chapman HN, Diederichs K, Messerschmidt M, Boutet S, Williams GJ, Marvin Seibert M, Caffrey M. 2015. Ternary structure reveals mechanism of a membrane diacylglycerol kinase. *Nat Commun* **6**:10140. doi:10.1038/ncomms10140

Li J, Xu H, West GM, Jones LH. 2016. Label-free technologies for target identification and validation. *Med Chem Commun* **7**:769–777. doi:10.1039/C6MD00045B

Lomenick B, Hao R, Jonai N, Chin RM, Aghajan M, Warburton S, Wang J, Wu RP, Gomez F, Loo JA, Wohlschlegel JA, Vondriska TM, Pelletier J, Herschman HR, Clardy J, Clarke CF, Huang J. 2009. Target identification using drug affinity responsive target stability (DARTS). *Proc Natl Acad Sci U S A* **106**:21984–21989. doi:10.1073/pnas.0910040106

Lyu J, Liu C, Zhang T, Schrecke S, Elam NP, Packianathan C, Hochberg GKA, Russell D, Zhao M, Laganowsky A. 2022. Structural basis for lipid and copper regulation of the ABC transporter MsbA. *Nat Commun* **13**:7291. doi:10.1038/s41467-022-34905-2

Martinez Molina D, Jafari R, Ignatushchenko M, Seki T, Larsson EA, Dan C, Sreekumar L, Cao Y, Nordlund P. 2013. Monitoring drug target engagement in cells and tissues using the cellular thermal shift assay **341**:84-7 doi: 10.1126/science.1233606.

Mateus A, Kurzawa N, Becher I, Sridharan S, Helm D, Stein F, Typas A, Savitski MM. 2020. Thermal proteome profiling for interrogating protein interactions. *Mol Syst Biol* **16**:e9232. doi:10.15252/msb.20199232

Molina DM, Jafari R, Ignatushchenko M, Seki T, Larsson EA, Dan C, Sreekumar L, Cao Y, Nordlund P. 2013. Monitoring Drug Target Engagement in Cells and Tissues Using the Cellular Thermal Shift Assay. *Science* **341**:84–87. doi:10.1126/science.1233606

O'Malley MA, Helgeson ME, Wagner NJ, Robinson AS. 2011. Toward rational design of protein detergent complexes: determinants of mixed micelles that are critical for the in vitro stabilization of a G-protein coupled receptor. *Biophys J* **19**:1938-48 doi: 10.1016/j.bpj.2011.09.018.

Ou X, Lao Y, Xu J, Wutthinitikornkit Y, Shi R, Chen X, Li J. 2021. ATP Can Efficiently Stabilize Protein through a Unique Mechanism. *JACS Au* **1**:1766–1777. doi:10.1021/jacsau.1c00316

Pai MY, Lomenick B, Hwang H, Schiestl R, McBride W, Loo JA, Huang J. 2015. Drug Affinity Responsive Target Stability (DARTS) for Small Molecule Target Identification. *Methods Mol Biol* **1263**:287–298. doi:10.1007/978-1-4939-2269-7_22

Pan Y, Zhan J, Jiang Y, Xia D, Scheuring S. 2023. A concerted ATPase cycle of the protein transporter AAA-ATPase Bcs1. *Nat Commun* **14**:6369. doi:10.1038/s41467-023-41806-5

Patel A, Malinovska L, Saha S, Wang J, Alberti S, Krishnan Y, Hyman AA. 2017. ATP as a biological hydrotrope. *Science* **356**:753–756. doi:10.1126/science.aaf6846

Perez-Perri JI, Ferring-Appel D, Huppertz I, Schwarzl T, Sahadevan S, Stein F, Rettel M, Galy B, Hentze MW. 2023. The RNA-binding protein landscapes differ between mammalian organs and cultured cells. *Nat Commun* **14**:2074. doi:10.1038/s41467-023-37494-w

Reinhard FBM, Eberhard D, Werner T, Franken H, Childs D, Doce C, Savitski MF, Huber W, Bantscheff M, Savitski MM, Drewes G. 2015. Thermal proteome profiling monitors ligand interactions with cellular membrane proteins. *Nat Methods* **12**:1129–1131. doi:10.1038/nmeth.3652

Santos R, Ursu O, Gaulton A, Bento AP, Donadi RS, Bologa CG, Karlsson A, Al-Lazikani B, Hersey A, Oprea TI, Overington JP. 2017. A comprehensive map of molecular drug targets. *Nat Rev Drug Discov* **16**:19–34. doi:10.1038/nrd.2016.230

Savitski MM, Reinhard FBM, Franken H, Werner T, Savitski MF, Eberhard D, Molina DM, Jafari R, Dovega RB, Klaeger S, Kuster B, Nordlund P, Bantscheff M, Drewes G. 2014. Tracking cancer drugs in living cells by thermal profiling of the proteome. *Science* **346**:1255784. doi:10.1126/science.1255784

Sharma S, Zhou R, Wan L, Feng S, Song K, Xu C, Li Y, Liao M. 2021. Mechanism of LolCDE as a molecular extruder of bacterial triacylated lipoproteins. *Nat Commun* **12**:4687. doi:10.1038/s41467-021-24965-1

Tang WK, Borgnia MJ, Hsu AL, Esser L, Fox T, de Val N, Xia D. 2020. Structures of AAA protein translocase Bcs1 suggest translocation mechanism of a folded protein. *Nat Struct Mol Biol* **27**:202–209. doi:10.1038/s41594-020-0373-0

The M and Kall L. 2020. Focus on the spectra that matter by clustering of quantification data in shotgun proteomics. *Nat Commun* **11**:3234 doi: 10.1038/s41467-020-17037-3.

Thompson RJ, Sayers I, Kuokkanen K, Hall IP. 2021. Purinergic Receptors in the Airways: Potential Therapeutic Targets for Asthma? *Front Allergy* **2**. doi:10.3389/falgy.2021.677677

Urner LH, Liko I, Pagel K, Haag R, Robinson CV. 2022. Non-ionic hybrid detergents for protein delipidation. *Biochimica et Biophysica Acta (BBA) - Biomembranes* **1864**:183958. doi:10.1016/j.bbamem.2022.183958

von Kügelgen I, Hoffmann K. 2016. Pharmacology and structure of P2Y receptors. *Neuropharmacology*, Special Issue: Purines in Neurodegeneration and Neuroregeneration **104**:50–61. doi:10.1016/j.neuropharm.2015.10.030

Yang Z, Wang C, Zhou Q, An J, Hildebrandt E, Aleksandrov LA, Kappes JC, DeLucas LJ, Riordan JR, Urbatsch IL, Hunt JF, Brouillette CG. 2014. Membrane protein stability can be compromised by detergent interactions with the extramembranous soluble domains. *Protein Sci* **23**:769–789. doi:10.1002/pro.2460

Ye Y, Li K, Ma Y, Zhang X, Li Y, Yu T, Wang Y, Ye M. 2023. The Introduction of Detergents in Thermal Proteome Profiling Requires Lowering the Applied Temperatures for Efficient Target Protein Identification. *Molecules* **28**:4859. doi:10.3390/molecules28124859

Young JW. 2023. Recent advances in membrane mimetics for membrane protein research. *Biochem Soc Trans* **51**:1405–1416. doi:10.1042/BST20230164

Zhan J, Zeher A, Huang R, Tang WK, Jenkins LM, Xia D. 2024. Conformations of Bcs1L undergoing ATP hydrolysis suggest a concerted translocation mechanism for folded iron-sulfur protein substrate. *Nat Commun* **15**:4655. doi:10.1038/s41467-024-49029-y

Zhang J, Zhang K, Gao Z-G, Paoletta S, Zhang D, Han GW, Li T, Ma L, Zhang W, Müller CE, Yang H, Jiang H, Cherezov V, Katritch V, Jacobson KA, Stevens RC, Wu B, Zhao Q. 2014. Agonist-bound structure of the human P2Y12 receptor. *Nature* **509**:119–122. doi:10.1038/nature13288

Zhang X, Ruan C, Zhu H, Li K, Zhang W, Wang K, Hu L, Ye M. 2020. A Simplified Thermal Proteome Profiling Approach to Screen Protein Targets of a Ligand. *PROTEOMICS* **20**:1900372. doi:10.1002/pmic.201900372

Zhao Z, Khurana A, Antony F, Young JW, Hewton KG, Brough Z, Zhong T, Parker SJ, Duong van Hoa F. 2023. A Peptidisc-Based Survey of the Plasma Membrane Proteome of a Mammalian Cell. *Mol Cell Proteomics* **22**:100588. doi:10.1016/j.mcpro.2023.100588

Zheng J, Jia Z. 2013. Tiny enzyme uses context to succeed. *Nature* **497**:445–446. doi:10.1038/nature12245

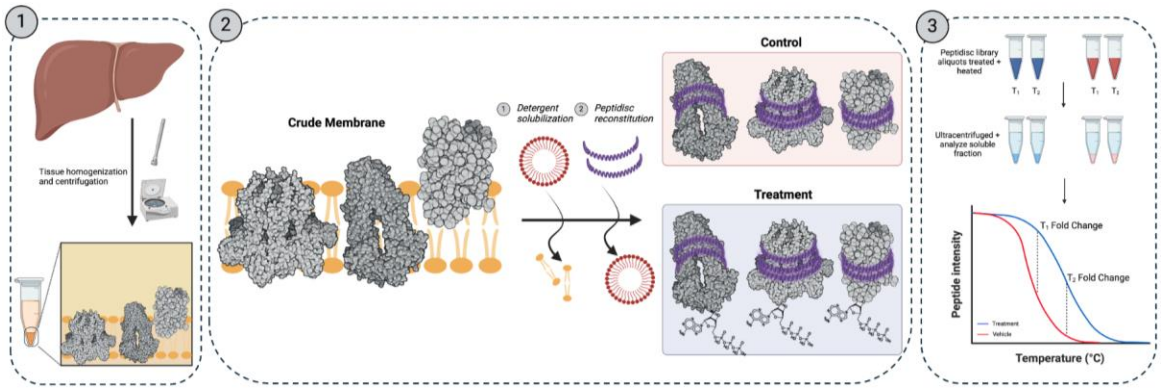

Figure 1: The Membrane Mimetic-Thermal Proteome Profiling (MM-TPP) experimental workflow. 1) Crude membranes are prepared from the liver organ. **2)** Integral membrane proteins (IMPs) are solubilized with detergent and reconstituted in the Peptidisc library. The water-soluble library is exposed to the ligand of interest (treatment) or the corresponding vehicle (control)**. 3)** Protein samples are heated at specific temperatures to induce precipitation, followed by ultracentrifugation. The soluble fraction is analyzed by mass spectrometry to detect changes in protein abundances between the treatment and control samples.

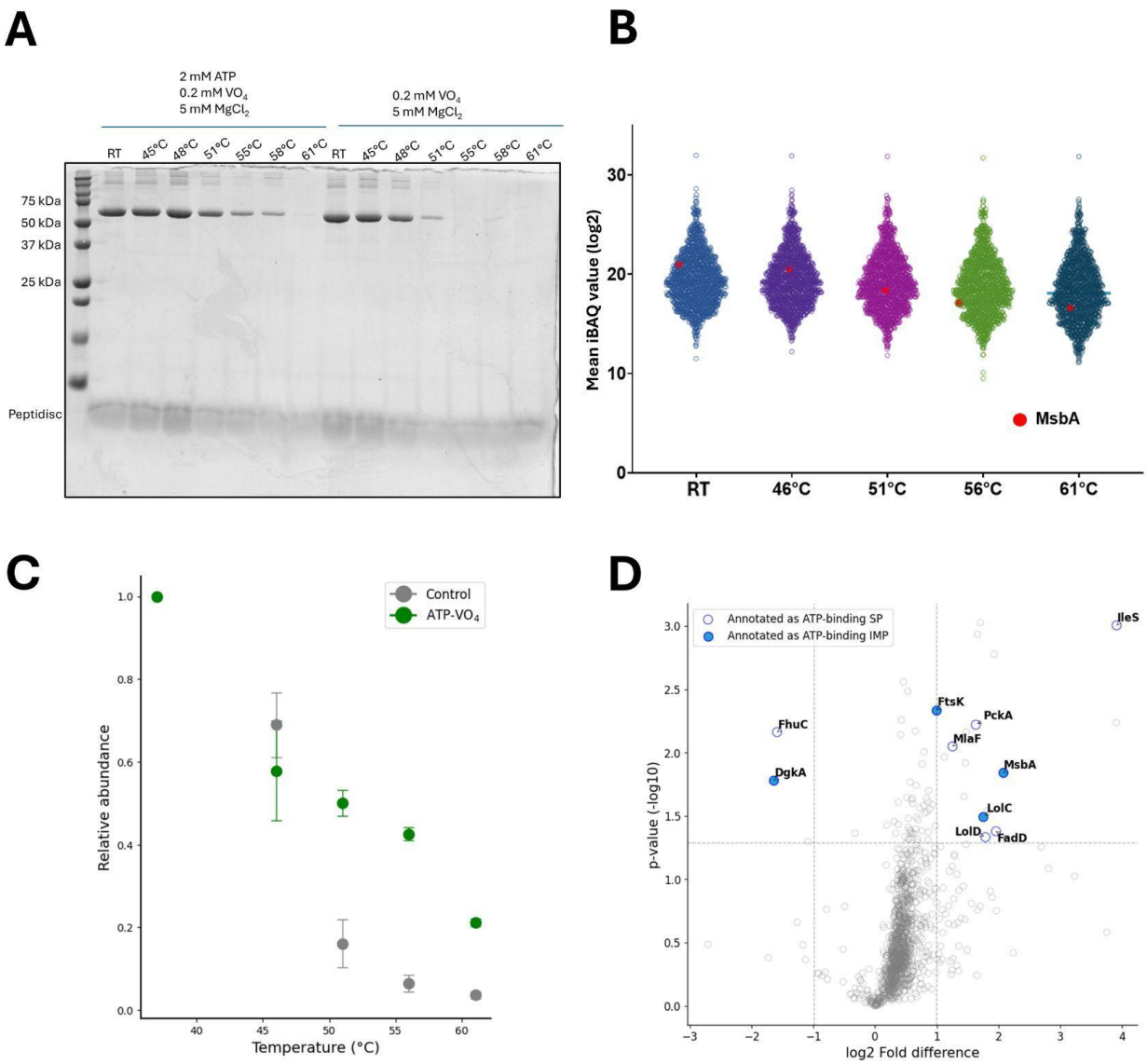

Figure 2: MM-TPP of integral membrane proteins (IMPs) prepared from *E. coli*.

(**A**) Stability of purified MsbA in Peptidisc in the presence of the indicated ligands. Samples are heat treated and centrifuged before analysis by 12% SDS-PAGE and Coomassie blue staining. (**B**) Grouped scatterplot representation of mean $\log_2$-transformed IBAQ value obtained for all identified proteins in the *E. coli* library at the indicated temperatures. The location of MsbA on

the plot is shown as a red dot. The mean value is obtained from three replicates of the temperature exposure assay (n = 3). (**C**) Relative abundance of MsbA based on the LFQ peptide intensities obtained across temperatures in the presence of ATP + orthovanadate (ATP-VO_4; orange) compared to a control sample (gray). Data is a mean ± standard deviation from triplicate assays (n = 3). **(D)** Volcano plot analysis of stabilized and destabilized proteins following ATP-VO_4 exposure at 61°C based on log_2-transformed LFQ peptide intensities. A log_2 fold difference significance cut-off of +1 and -1 with a $-log_{10}$ p-value cut-off of $p > 1.3$ is applied. Hollow blue dots indicate annotated ATP-binding soluble proteins (SP) and solid blue dots indicate ATP-binding integral membrane proteins (IMPs). Data represent the mean from three replicates (n = 3).

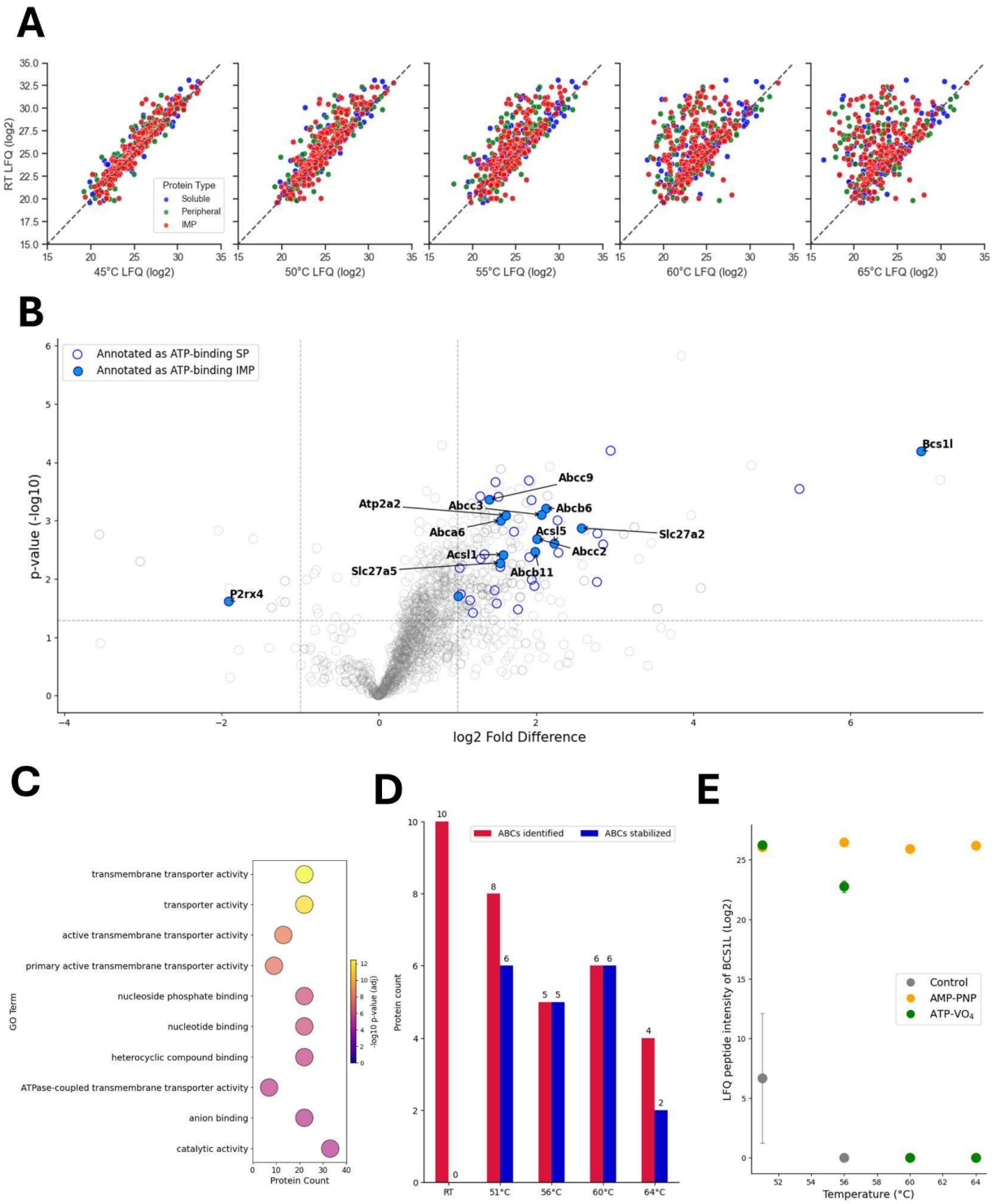

Figure 3: MM-TPP of integral membrane proteins (IMPs) prepared from the mouse liver tissue.

(**A**) Global protein intensities derived from log_2-transformed LFQ values of peptidisc-reconstituted liver extract. The plot displays soluble proteins (blue), membrane-associated (green), and IMPs (red) identified at the indicated temperatures compared to room temperature (RT). The dashed line is the identical value line. (**B**) Volcano plot of stabilized and destabilized proteins based on log_2-transformed LFQ values at 51 °C based on a fold difference cutoff of > 1 or < -1 and $-log_{10}$ p-value of > 1.3. The soluble proteins (SP) annotated as ATP-binding are represented as hollow blue circles, and the IMPs annotated as ATP-binding are represented as solid blue circles. The mean value is obtained from three replicates at the temperature exposure assay (n = 3). (**C**) GO-term enrichment analysis of molecular functions of stabilized IMPs identified in B. The presented top 10 significant terms are based on adjusted p-value (FDR = 5% after Benjamini-Hochberg correction) (**D**) Number of ATP-binding cassette (ABC) transporters identified and stabilized by ATP-VO_4 at the indicated temperatures. (**E**) Log_2 transformed LFQ Peptide intensities of BCS1L in the presence of ATP-VO_4 (green), AMP-PNP (orange), and vehicle control (gray) across the temperature range. Data is a mean ± standard deviation from three replicates (n = 3).

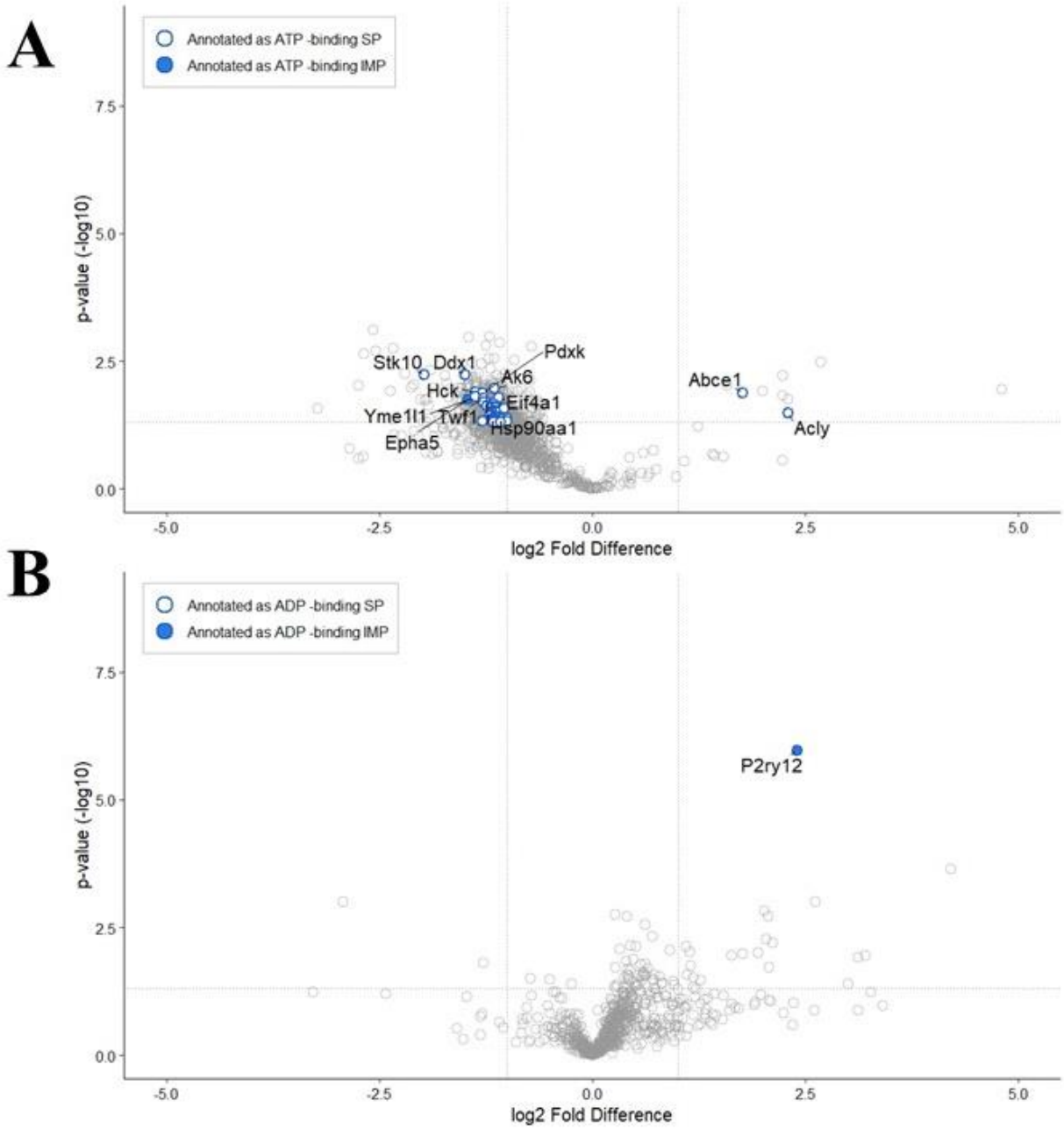

Figure 4: Protein Stabilization Profiles at 51 °C with ATP–VO_4 in DB-TPP and 2-MeS-ADP in MM-TPP.

(A) Volcano plot of stabilized and destabilized proteins at 51 °C in detergent-based TPP (DB-TPP) with ATP-VO_4. Log_2-transformed LFQ peptide values were used, with thresholds set at a fold-change > 1 or < –1 and a $–log_{10}$ p-value > 1.3. Soluble proteins (SP) annotated as ATP-binding are shown as hollow blue circles, and integral membrane proteins (IMPs) annotated as ADP-binding are shown as solid blue circles. Data represent the mean of three biological replicates (n = 3).

(B) Volcano plot of stabilized and destabilized proteins at 51 °C in MM-TPP with 2-methylthio-ADP (2-MeS-ADP), displayed using the same thresholds and annotations as in panel A.

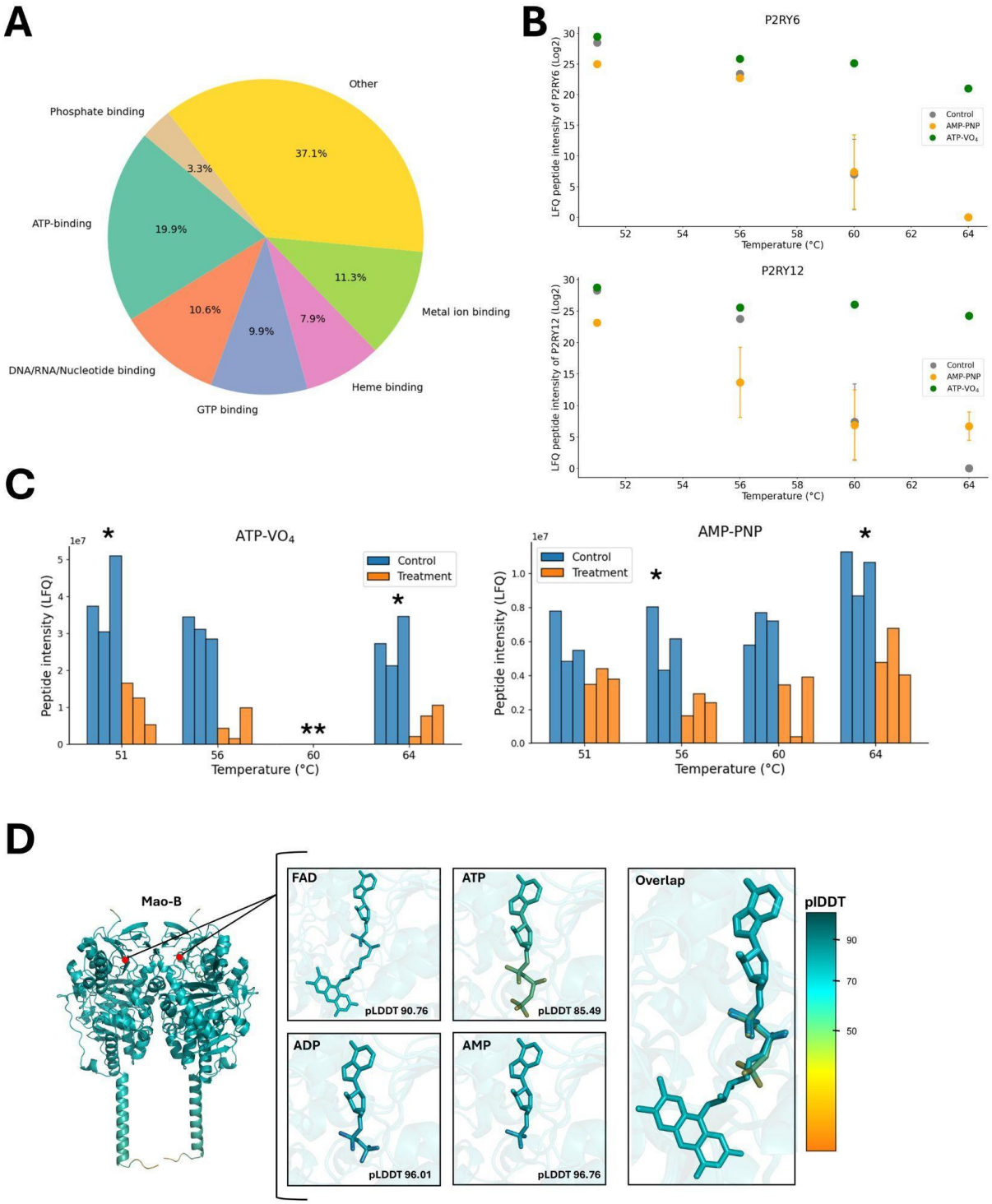

Figure 5: ATP and Analogue-Induced Off-Target Stabilization of Liver Membrane Proteins.

(**A**) GO-term analysis of molecular functions and distribution for all IMPs (n= 178) significantly stabilized with ATP-VO_4 at temperatures tested with the mouse liver library. (**B**) Log_2 transformed LFQ Peptide intensity variations of P2RY6 and P2RY12 over the temperature range with AMP-PNP (orange), ATP-VO_4 (green), or none (gray). Data is a mean ± standard deviation from three replicates (n = 3). **(C)** Relative LFQ Peptide intensity variations of P2RX4 at the indicated temperature in the presence of ATP-VO_4 (left panel) or AMP-PNP (right panel). Data from treatment samples (orange) and control samples (blue) is from triplicates (n = 3). * Represents p-value ≤ 0.05. **Protein not detected. (**D**) Structural model of homodimeric Mao-B with the predicted binding of FAD, ATP, ADP, and AMP ligands within the FAD binding pocket, indicated as red dots. Each ligand is presented individually in the FAD binding pocket or as an all-ligand overlap generated by *AlphaFold3*. The respective Predicted Local Distance Difference Test (pLDDT) score for each ligand is shown, with higher scores representing more favourable ligand fitting. The colour gradient represents a high pLDDT score as blue and a low pLDDT score as orange.

Uniprot-ID	Protein Name	Full protein name	Stabilized temperatures (°C)
Q8K441	ABCA6	ATP-binding cassette sub-family A member 6	51, 56, 60, 64
J3QNY6	ABCB11	ATP-binding cassette, sub-family B (MDR/TAP), member 11	51, 56, 60
Q9DC29	ABCB6	ATP-binding cassette sub-family B (MDR/TAP), member 6	51
Q8VI47	ABCC2	ATP-binding cassette sub-family C (CFTR/MRP), member 2	51, 56, 60
A0A0R4J015	ABCC3	ABC-type glutathione-S-conjugate transporter (CFTR/MRP)	51, 60
P70170	ABCC9	ATP-binding cassette sub-family C member 9 (Sulfonylurea receptor 2)	51, 56, 60
S4R2E1	ABCG2	ATP-binding cassette sub-family G member 2) (Urate exporter)	56, 60, 64
Q99PE8	ABCG5	ATP-binding cassette sub-family G member 5 (Sterolin-1)	51

Table 1: ATP-binding cassette transporters detected in the mouse liver Peptidisc library. A minimum of two unique peptides was required to identify the protein at a given temperature. The exact number of unique peptides identified for each protein under each ligand and temperature condition is provided in **Supplemental Table 2**. Stabilization was defined using a $\log_2$ fold change > 1 between treatment and control samples, with a -log10 p > 1.3, calculated from replicate samples (n = 3).

	MM-TPP				DB-TPP			
			SPs	IMPs			SPs	IMPs
Temperature (°C)	Total Protein	IMPs	% ATP binders stabilized	% ATP binders stabilized	Total Protein	IMPs	% ATP binders stabilized	% ATP binders stabilized
51	1380	419 (30%)	33.7%	37.9%	1862	428 (23%)	1.74%	0%
56	1179	369 (31%)	39.2%	45.6%	1839	428 (23%)	0%	0%
60	1090	344 (32%)	22.9%	48.4%	1621	391 (24%)	0%	0%
64	992	316 (32%)	47.0%	58.1%	1539	372 (24%)	0%	5.56%

Table 2: Comparison of ATP-Binding Protein Stabilization in MM-TPP and DB-TPP. Reported values at each temperature represent the total number of proteins meeting the inclusion criteria (at least 2 unique peptides) across triplicate control and treatment conditions. As protein counts are determined post-analysis, they are reported as single values rather than as means with standard deviations. Each protein was identified based on at least two unique peptides (n = 3).

Supplementary Figures

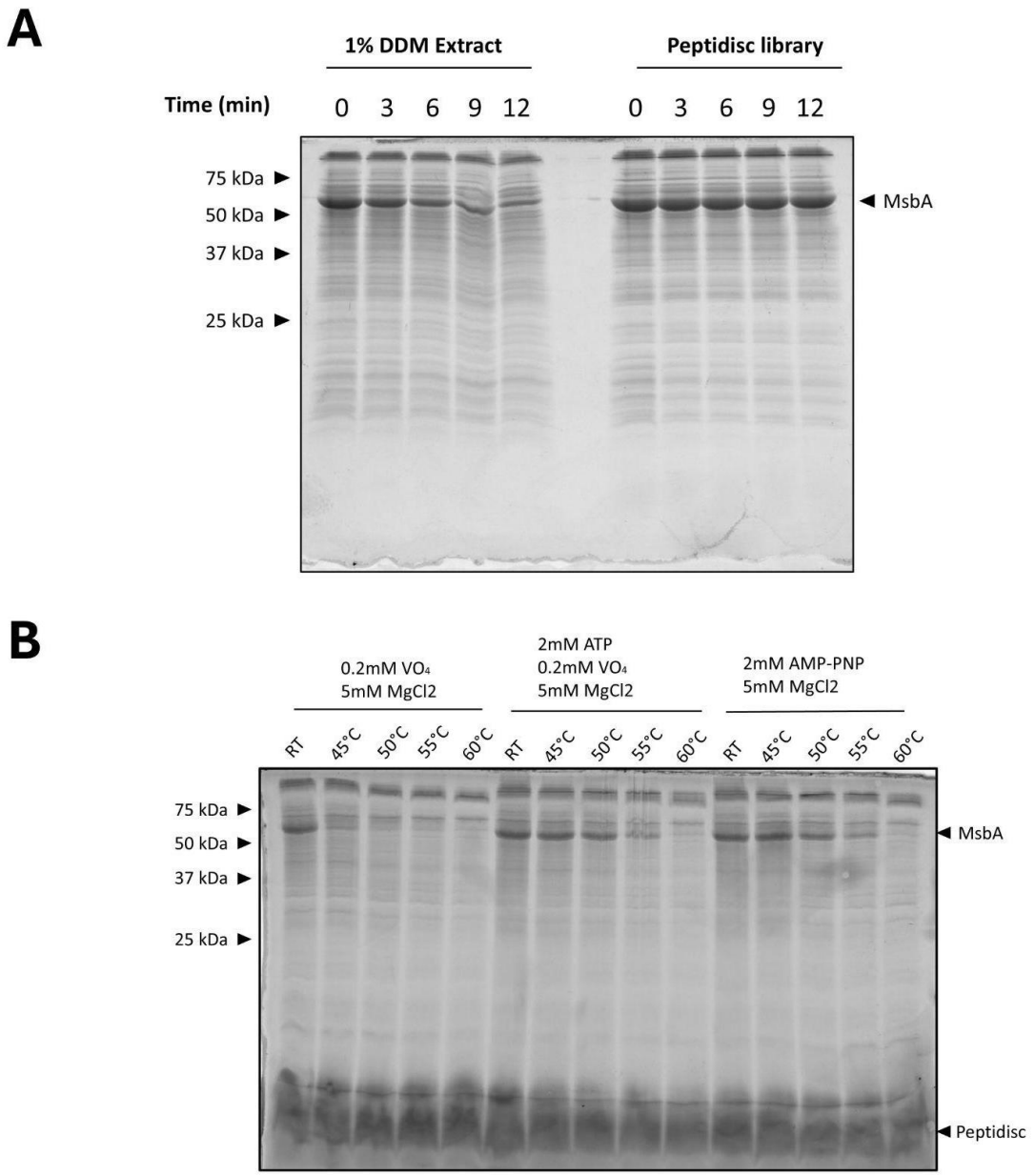

Supplementary Figure 1: Thermal stability of MsbA in detergent and in Peptidisc with different ligands.

(**A**) The *E. coli* membrane fraction enriched for MsbA was solubilized with 1% DDM or reconstituted in Peptidisc. The detergent extract and Peptidisc library were incubated at 45°C for the indicated times. After ultra-centrifugation, the supernatants were analyzed on 15% SDS-PAGE and visualized with Coomassie blue staining. (**B**) The Peptidisc library prepared in (A) was incubated with ATP-VO_4 or AMP-PNP at the indicated temperature. After ultra-centrifugation, the supernatants were analyzed on 15% SDS-PAGE and visualized with Coomassie blue staining.

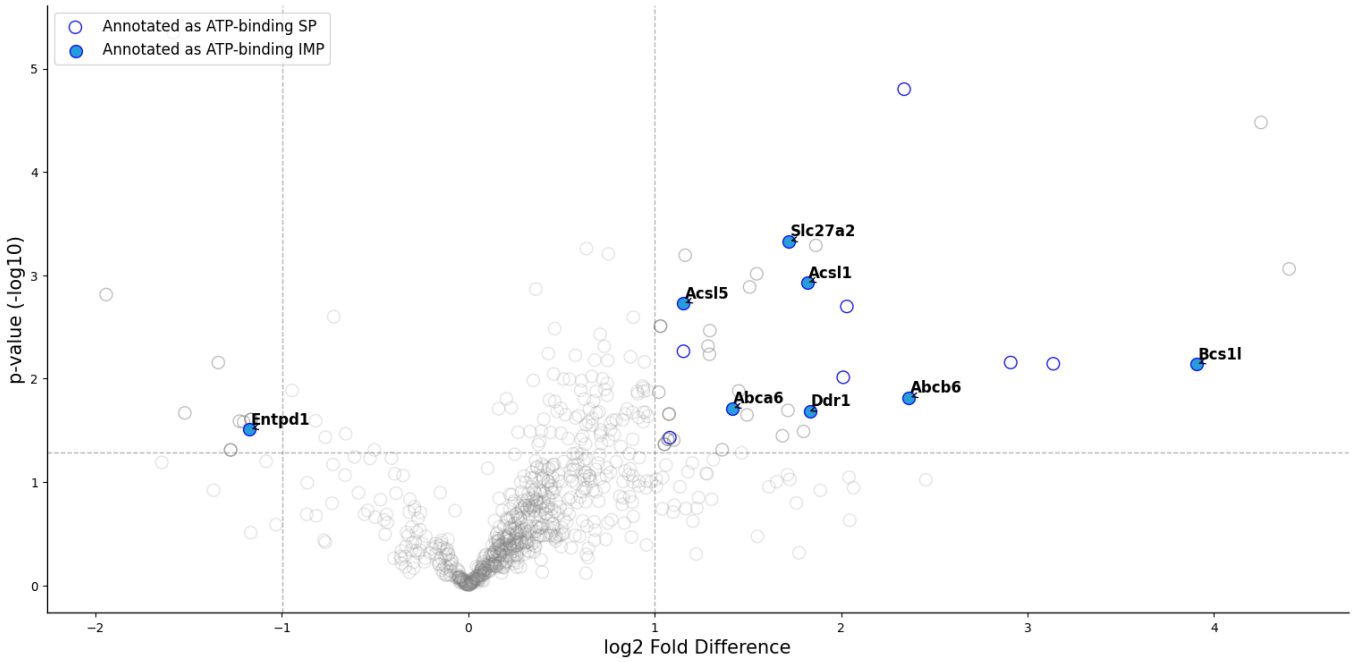

Supplementary Figure 2: Volcano plot of stabilized and destabilized proteins at 51 °C in the presence of AMP-PNP.

Soluble proteins (SP) annotated as ATP-binding proteins are presented as hollow blue circles, and IMPs annotated as ATP-binding are presented as solid blue circles. Values taken from log_2-

transformed LFQ peptide intensities. The mean value is obtained from three replicates at the temperature exposure assay (n = 3).

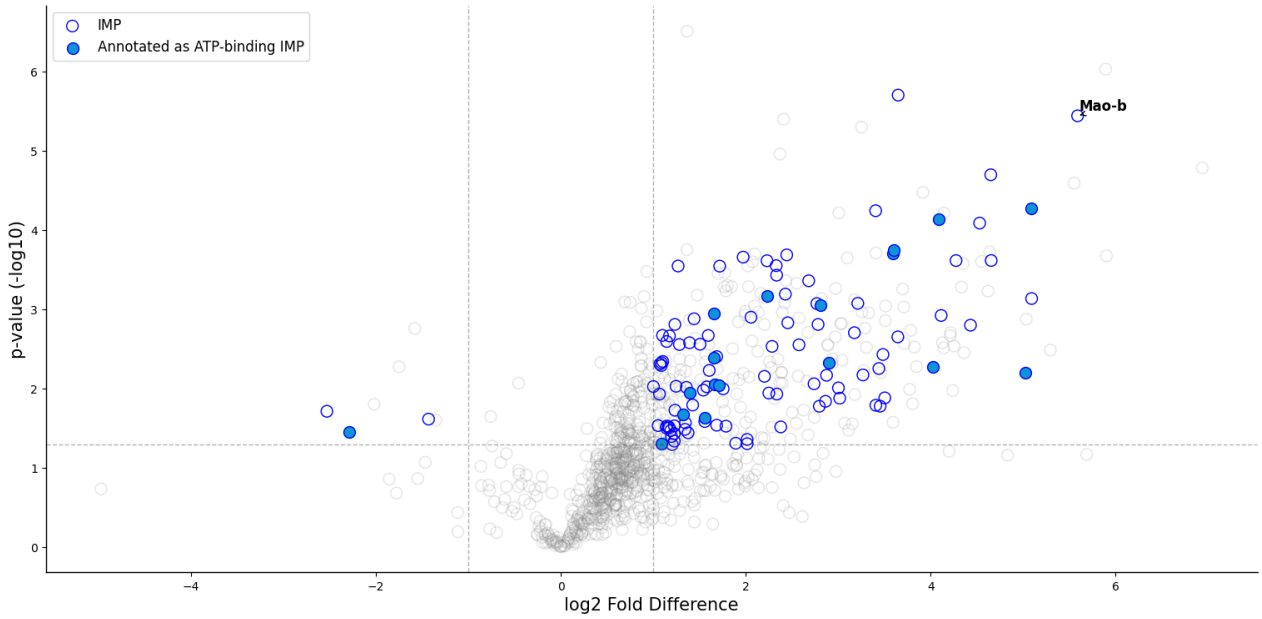

Supplementary Figure 3: Volcano plot of stabilized and destabilized proteins at 64 °C in the presence of ATP-VO_4.

IMPs are represented by hollow blue circles and IMPs annotated as ATP-binding are represented by solid blue circles. Values taken from log_2-transformed LFQ peptide intensities. The mean value is obtained from three replicates at the temperature exposure assay (n = 3).

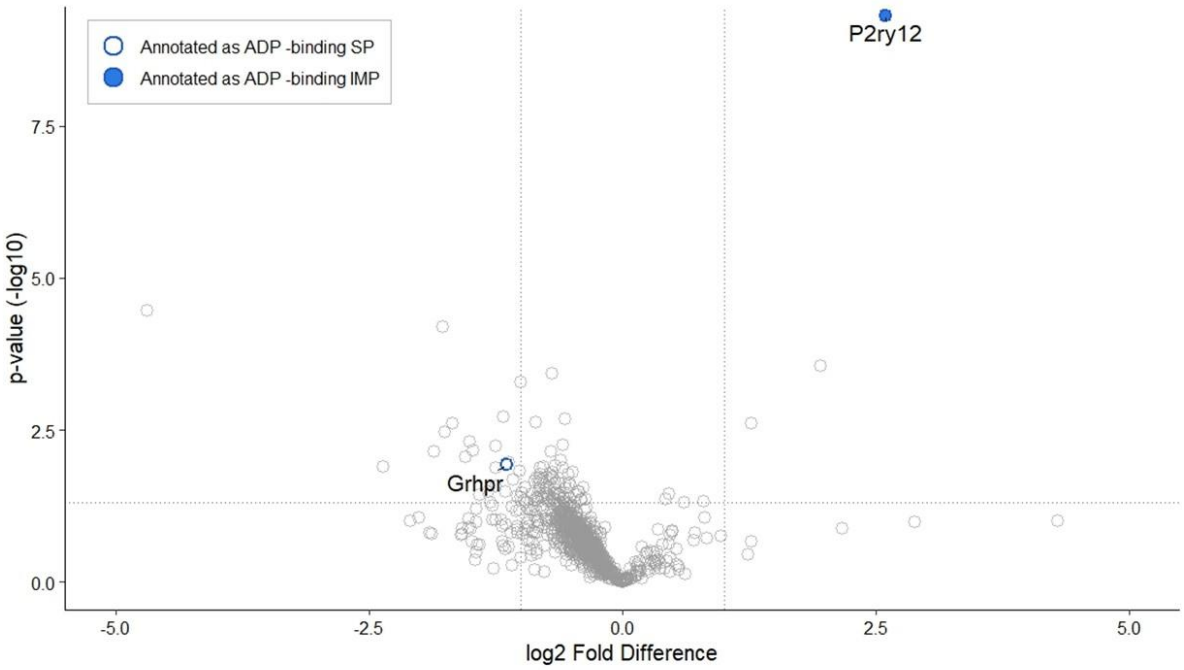

Supplementary Figure 4: Volcano plot of stabilized and destabilized proteins at 57 °C in the presence of 2-MeS-ADP.

The soluble proteins (SP) annotated as ADP-binding are represented by hollow blue circles and the IMPs annotated as ADP-binding are represented by solid blue circles. Values taken from log_2-transformed LFQ peptide intensities. The mean value is obtained from three replicates at the temperature exposure assay (n = 3).

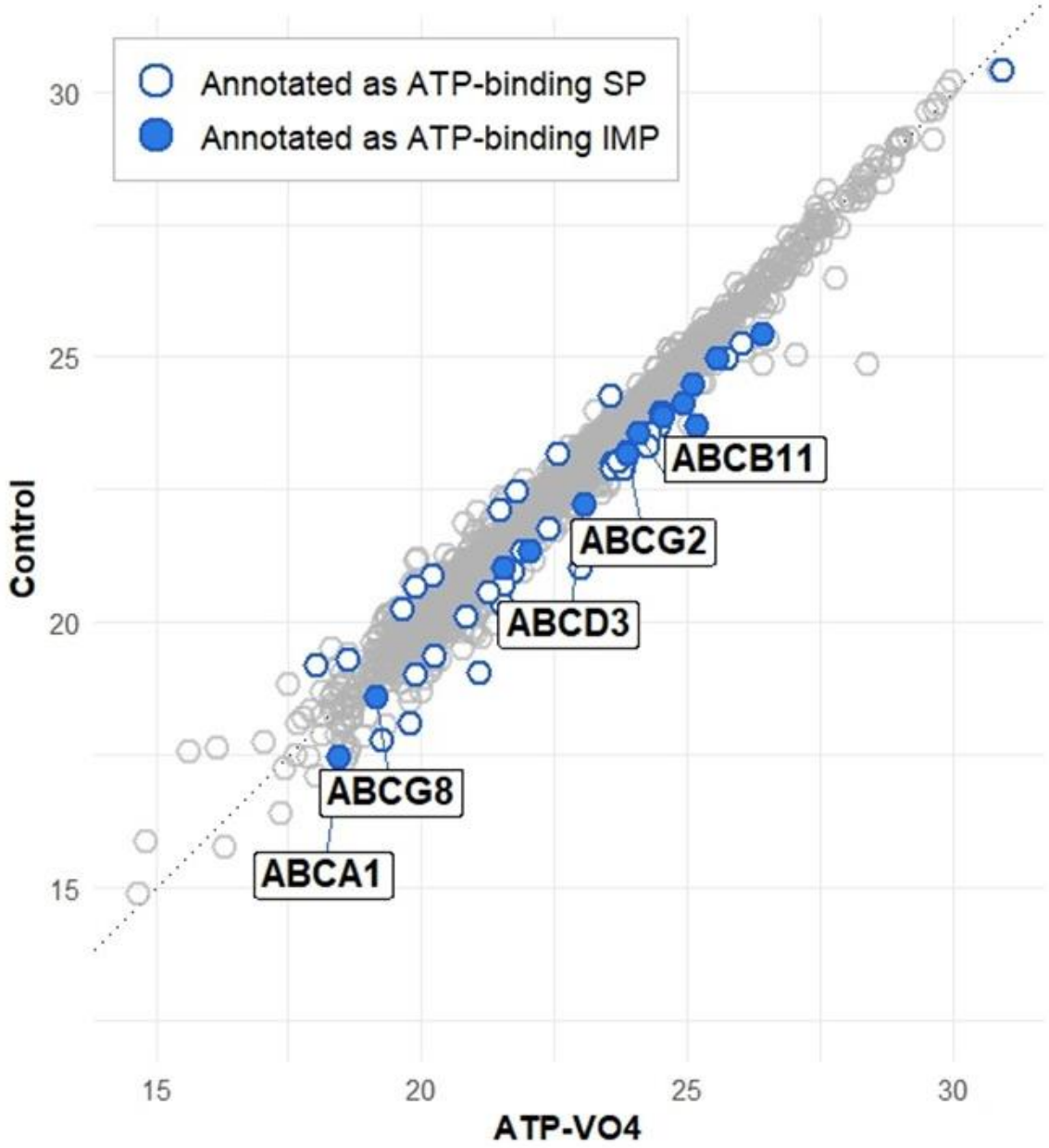

Supplementary Figure 5: Correlation plot of protein differential stabilization at 51 °C in MM-TPP, performed with DIA data acquisition from a whole mouse liver library. ATP-binding proteins with $|\log_2 \text{ fold change}| \geq 0.5$ are highlighted. Soluble proteins (SP) annotated as ATP-binding are shown as hollow blue circles, while IMPs annotated as ATP-binding are shown

as solid blue circles. ABC transporters that pass the significance threshold are labeled on the plot.

Temperature	Total protein	Total IMP
Room temperature	998 ± 2	470 ± 3 (47%)
45°C	892 ± 11	425 ± 1 (48%)
50°C	810 ± 16	385 ± 7 (48%)
55°C	734 ± 46	354 ± 22 (48%)
60°C	566 ± 33	276 ± 11 (49%)
65°C	524 ± 4	264 ± 3 (50%)

Supplemental Table 1: Total and Integral Membrane Protein Counts Across Temperatures in Mouse Liver Peptidisc Libraries. The % value is used to assess IMP loss relative to total protein count. Each protein was identified based on at least two unique peptides (n = 2)

Target	Treatment	Number of unique peptides			
		51 °C	**56/57 °C**	**60/61 °C**	**64 °C**
MsbA	ATP–VO_4	Control: 13,12,6	Control:11,4,9	Control:7,5,6	

		Treatment: 16,16,15	Treatment:17,15,17	Treatment: 14,11,14	
ABCA6	ATP–VO_4	Control: 9,12,13	Control:5,3,6	Control:1,0,3	Control:1,0,0
		Treatment:21,19,23	Treatment:12,15,17	Treatment:12,13,11	Treatment:7,7,9
	ATP–VO_4 (DB-TPP)	Control:22,25,25	Control:25,27,23	Control:22,23,22	Control:14,19,15
		Treatment:25,25,24	Treatment:22,24,23	Treatment:17,5,22	Treatment:13,20,15
	2-MeS-ADP	Control:6,5,5	Control:0,1,0		
		Treatment:1,5,7	Treatment:2,2,1		
	AMP-PNP	Control:6,5,5	Control:3,1,5	Control:1,2,3	Control:0,0,0
		Treatment:6,7,6	Treatment:3,6,4	Treatment:2,0,1	Treatment:0,0,0
ABCB11	ATP–VO_4	Control:13,10,15	Control:0,3,4	Control:1,0,0	Control:0,1,0
		Treatment:21,22,21	Treatment:6,13,12	Treatment:6,10,9	Treatment:1,2,3
	ATP–VO_4 (DB-TPP)	Control:30,32,29	Control:26,25,27	Control:22,20,24	Control:16,15,16
		Treatment:38,37,38	Treatment:30,32,23	Treatment:20,5,19	Treatment:15,23,17
	2-MeS-ADP	Control:0,0,0	Control:0,0,0		
		Treatment:0,0,0	Treatment:0,0,0		
	AMP-PNP	Control:6,6,5	Control:1,2,3	Control:1,2,1	Control:0,0,0

		Treatment:8,8,7	Treatment:7,3,4	Treatment:2,0,4	Treatment:0,0,0
ABCB6	ATP–VO_4	Control:0,1,1	Control:0,0,0	Control:0,0,0	Control:0,0,0
		Treatment:3,3,3	Treatment:0,0,0	Treatment:0,0,0	Treatment:0,0,0
	ATP–VO_4 (DB-TPP)	Control:0,0,0	Control:0,0,0	Control:0,0,0	Control:0,0,0
		Treatment:0,0,0	Treatment:0,0,0	Treatment:	Treatment:0,0,0
	2-MeS-ADP	Control:0,0,0	Control:0,0,0		
		Treatment:0,0,0	Treatment:0,0,0		
	AMP-PNP	Control:0,0,0	Control:0,0,0	Control:0,0,0	Control:0,0,0
		Treatment:3,2,2	Treatment:2,2,2	Treatment:0,0,0	Treatment:0,0,0
ABCC2	ATP–VO_4	Control:6,4,9	Control:0,0,0	Control:0,0,0	Control:0,0,0
		Treatment:13,15,10	Treatment:6,6,5	Treatment:3,5,2	Treatment:0,0,0
	ATP–VO_4 (DB-TPP)	Control:13,15,15	Control:16,11,12	Control:8,10,8	Control:3,3,5
		Treatment:22,19,16	Treatment:17,16,15	Treatment:7,6,11	Treatment:8,12,6
	2-MeS-ADP	Control:2,2,4	Control:0,0,0		
		Treatment:3,1,6	Treatment:1,2,1		
	AMP-PNP	Control:1,1,3	Control:0,0,0	Control:0,0,0	Control:0,0,0
		Treatment:4,3,2	Treatment:0,0,0	Treatment:0,0,0	Treatment:0,0,0

ABCC3	ATP–VO_4	Control:10,6,7	Control:0,0,0	Control:0,0,0	Control:0,0,0
		Treatment:13,15,15	Treatment:0,0,0	Treatment:2,3,5	Treatment:0,0,0
	ATP–VO_4 (DB-TPP)	Control:0,0,0	Control:0,0,0	Control:0,0,0	Control:0,0,0
		Treatment:0,0,0	Treatment:0,0,0	Treatment:0,0,0	Treatment:0,0,0
	2-MeS-ADP	Control:0,0,0	Control:0,0,0		
		Treatment:0,0,0	Treatment:0,0,0		
	AMP-PNP	Control:0,0,0	Control:0,0,0,	Control:0,0,0	Control:0,0,0
		Treatment:0,0,0	Treatment:0,0,0	Treatment:0,0,0	Treatment:0,0,0
ABCC9	ATP–VO_4	Control:15,14,13	Control:6,5,6	Control:2,0,4	Control:1,0,2
		Treatment:15,16,17	Treatment:5,8,9	Treatment:7,13,10	Treatment:8,7,6
	ATP–VO_4 (DB-TPP)	Control:1,1,1	Control:1,1,1	Control:1,1,1	Control:1,1,1
		Treatment:1,1,1	Treatment:1,1,1	Treatment:1,1,1	Treatment:1,1,1
	2-MeS-ADP	Control:16,19,18	Control:6,8,3		
		Treatment:15,18,20	Treatment:3,12,8		
	AMP-PNP	Control:13,12,11	Control:5,7,7	Control:5,9,6	Control:4,3,6
		Treatment:13,13,13	Treatment:11,9,9	Treatment:7,3,8	Treatment:3,5,4

ABCG2	ATP–VO_4	Control:6,8,9	Control:6,6,5	Control:2,0,1	Control:0,0,1
		Treatment:8,7,9	Treatment:8,8,7	Treatment:9,8,7	Treatment:4,5,5
	ATP–VO_4 (DB-TPP)	Control:10,11,11	Control:9,9,10	Control:5,7,6	Control:4,4,4
		Treatment:10,11,12	Treatment:10,10,7	Treatment:3,1,5	Treatment:2,6,4
	2-MeS-ADP	Control:4,3,3	Control:1,1,0		
		Treatment:3,3,3	Treatment:0,1,0		
	AMP-PNP	Control:3,3,3	Control:1,0,0	Control:0,0,0	Control:0,0,0
		Treatment:3,3,3	Treatment:3,3,3	Treatment:3,2,3	Treatment:0,0,0
ABCG5	ATP–VO_4	Control:1,1,1	Control:0,0,0	Control:0,0,0	Control:0,0,0
		Treatment:2,2,2	Treatment:0,0,0	Treatment:0,0,0	Treatment:0,0,0
	ATP–VO_4 (DB-TPP)	Control:2,1,2	Control:1,1,1	Control:0,0,0	Control:0,0,0
		Treatment:2,2,1	Treatment:1,0,1	Treatment:0,0,0	Treatment:0,0,0
	2-MeS-ADP	Control:0,0,0	Control:0,0,0		
		Treatment:0,0,0	Treatment:0,0,0		
	AMP-PNP	Control:0,0,0	Control:0,0,0	Control:0,0,0	Control:0,0,0
		Treatment:0,0,0	Treatment:0,0,0	Treatment:0,0,0	Treatment:0,0,0

BCS1l	ATP–VO_4	Control: 0,0,0	Control:0,0,0	Control: 0,0,0	Control: 0,0,0
		Treatment: 6,7,6	Treatment: 1,4,2	Treatment:0,0,0	Treatment: 1,0,0
	ATP–VO_4 (DB-TPP)	Control: 1,4,4	Control:1,0,1	Control: 0,0,0	Control: 0,0,0
		Treatment: 7,5,4	Treatment: 0,2,3	Treatment: 0,0,0	Treatment: 1,0,0
	2-MeS-ADP	Control: 0,0,0	Control: 0,0,0		
		Treatment:,0,0,0	Treatment: 0,0,0		
	AMP-PNP	Control: 0,0,1	Control:0,0,0	Control:0,0,0	Control:0,0,0
		Treatment:13.10.12	Treatment:15,15,15	Treatment:15,4,12	Treatment:16,13,9
P2RX4	ATP–VO_4	Control: 3, 2, 3	Control: 3,3,2	Control: 0,0,0	Control:3,4,5
		Treatment: 3,3,1	Treatment:1,0,1	Treatment: 0,0,0	Treatment:0,1,3
	ATP–VO_4 (DB-TPP)	Control: 3,1,4	Control: 2,3,2	Control: 4,3,3	Control:1,1,2
		Treatment:2,1,1	Treatment: 1,1,2	Treatment:1,2,2	Treatment: 1,2,2
	2-MeS-ADP	Control: 0,0,0	Control: 0,0,0		
		Treatment: 0,0,0	Treatment: 0,0,0		
	AMP-PNP	Control:2,2,2	Control:2,2,2	Control:2,2,2	Control:2,2,2
		Treatment:2,1,2	Treatment:2,1,1	Treatment:2,0,2	Treatment:2,2,2

P2RY6	ATP–VO_4	Control: 12, 13, 13	Control:2.2.3	Control:1,0,0	Control:0,0,0
		Treatment:12,10,13	Treatment:3,5,6	Treatment:2,4,3	Treatment:0,0,0
	ATP–VO_4 (DB-TPP)	Control: 22,22,22	Control: 4,2,3	Control:0,0,1	Control: 0,1,0
		Treatment: 25,23,25	Treatment: 3,1,5	Treatment: 0,0,1	Treatment: 1,0,0
	2-MeS-ADP	Control: 2,2,2	Control: 1,1,0		
		Treatment: 0,2,2	Treatment: 1,1,1		
	AMP-PNP	Control:7,5,6	Control:1,0,0	Control:0,0,0	Control: 0,0,0
		Treatment:8,8,4	Treatment:1,2,3	Treatment: 0,0,0	Treatment: 0,0,0
P2RY12	ATP–VO_4	Control:19,15,15	Control:2,5,4	Control:0,0,1	Control:0,0,0
		Treatment:14,14,13	Treatment:3,6,9	Treatment: 8,9,8	Treatment: 5,4,5
	ATP–VO_4 (DB-TPP)	Control:29, 30, 30	Control: 22, 21, 25	Control: 20, 16, 18	Control:14, 12, 14
		Treatment:29, 28, 29	Treatment: 23, 21, 23	Treatment: 19,11,17	Treatment:13,16,14
	2-MeS-ADP	Control: 6,4,7	Control: 2,3,4		
		Treatment: 7,6,7	Treatment: 4,3,6		
	AMP-PNP	Control:2,1,2	Control:0,0,0	Control:0,0,0	Control:0,0,0
		Treatment:3,2,2	Treatment:0,0,0	Treatment:0,0,0	Treatment:0,0,0

Mao-B	ATP–VO_4	Control:20,18,18	Control:15,14,14	Control:14,0,13	Control:1,1,1
		Treatment:20,21,20	Treatment:16,14,17	Treatment:14,17,18	Treatment:14,15,15
	ATP–VO_4 (DB-TPP)	Control:25,24,26	Control:25,24,27	Control:21,19,21	Control:15,15,18
		Treatment:26,23,26	Treatment:25,21,21	Treatment:17,6,19	Treatment:14,17,18
	2-MeS-ADP	Control:23,21,22	Control:20,17,17		
		Treatment:18,24,24	Treatment:20,18,19		
	AMP-PNP	Control:15,17,16	Control:10,13,13	Control:13,13,14	Control:8,9,8
		Treatment:17,17,17	Treatment:15,12,13	Treatment:10,10,14	Treatment:10,9,7

Supplemental Table 2: Unique peptide counts for proteins highlighted in this study.

MsbA, ABCA6, ABCB1, ABCB6, ABCC2, ABCC3, ABCC9, ABCG2, ABCG5, BCS1L, P2RX4, P2RY6, P2RY12, and MAO-B. Counts are from MaxQuant analyses using a data-dependent acquisition (DDA) workflow across the temperatures tested in MM-TPP (with ATP–VO_4, 2-MeS-ADP, and AMP-PNP) and in DB-TPP (with ATP–VO_4).